https://doi.org/10.5194/egusphere-2026-3783
Preprint. Discussion started: 20 August 2026

SEMPAS: A UV-visible Spectroscopy Instrument for Monitoring Shipping Emissions and Atmospheric Composition on the North Sea

Gytha Mettepenningen[1,3], Caroline Fayt[1], Cato Van Doorne[1], Aurélien Aubry[1], Sophie Berkenbosch[1], Martine De Mazière[1], Filip Desmet[1], Lars Jacobs[1], Eddy Neefs[1], Frederik Tack[1], Timo Van Laar[1], Clemens Mensink[2,3], and Michel Van Roozendael[1]

[1]Royal Belgian Institute for Space Aeronomy (BIRA-IASB), Ringlaan 3, 1180 Ukkel, Belgium
[2]Vlaams Instituut voor Technologisch Onderzoek (VITO), Boeretang 200, 2400 Mol, Belgium
[3]Ghent University, Dept. of Physics & Astronomy, Krijgslaan 281, B-9000 Ghent, Belgium

Correspondence: Gytha Mettepenningen (gytha.mettepenningen@aeronomie.be)

Abstract. Ship emissions contribute significantly to global transport pollution, foremost NO_x and SO_x. To mitigate this issue, emission regulated areas have been established, such as in the North Sea. Monitoring systems are essential to ensure consistent compliance to the emission limits. The Ship Emission Monitoring with Passive Absorption Spectroscopy (SEMPAS) instrument has been developed to provide operational monitoring of individual ships; as they transit past the instrument's on-shore or off-shore installation location. SEMPAS applies the UV-visible Differential Optical Absorption Spectroscopy (DOAS) technique to identify SO_2 and NO_2 in the UV, serving as qualitative proxies for NO_x and SO_x emissions. Through an optical fiber bundle organised as a matrix, a coarse 2D scene of the ship plume is captured. Robust housing protects the hardware from the marine environment. The instrument is equipped with a camera, coupled with image recognition software and an Automatic Identification System (AIS) receiver to identify individual ships. The vessels are actively tracked along their trajectory, to perform multiple consecutive measurements of a single ship. In the absence of nearby ships, the instrument operates as a Multi-Axis (MAX-)DOAS system providing regular measurements of the vertical profiles of NO_2 and HCHO. These can be used for atmospheric composition research, as well as satellite validation in a marine environment. In this study, first shipping results are presented from a test campaign in Zeebrugge, Belgium. The ship tracking algorithm is stable, while NO_2 and SO_2 measurements show large variations. A good agreement is found between MAX-DOAS measurements and satellite observations, with discrepancies dominated by local emissions from the port environment.

1 Introduction

Emissions from ship traffic are increasing rapidly: They account for up to 15% of global transport pollution (Manshausen et al., 2022; Eyring et al., 2005). This presents a hazard for air quality and human health, especially in densely inhabited coastal regions (Aulinger et al., 2016; Yang et al., 2016). To mitigate this impact, accurate monitoring of shipping emissions is essential. In densely populated water zones such as the North Sea, ship emissions for NO_x and SO_x are regulated by the International Maritime Organisation (IMO), through Nitrogen Emission Controlled Areas (NECAs) and Sulphur Emission Controlled Areas (SECAs) (MEPC, 2025). Thresholds are set for individual ships sailing in this area.

https://doi.org/10.5194/egusphere-2026-3783
Preprint. Discussion started: 20 August 2026

To limit SO_x emissions in SECA zones, the amount of sulphur contained in the fuel oil (Fuel Sulphur Content, FSC) is currently limited to 0.1% (MEPC, 2022). The NO_x limits in NECA zones are more complex and depend on the age, engine, and engine rated speed of the ship. Regulations become increasingly stringent for ships constructed after a specified year (MEPC, 2008; Cheng et al., 2017). The introduction of control zones has shown an increase in ships operating on less-polluting fuel; however, in the absence of adequate monitoring, compliance levels are likely to decline (Moreira et al., 2024; Repka et al., 2021).

After the SECA standards tightened in 2015, the maximum permitted FSC was reduced from 1% to 0.1%. This stricter limit is associated with a substantial reduction in ship-related SO_2 emissions. As a consequence, a low detection limit becomes critical for newly developed monitoring instruments. In the Belgian North Sea, the current method of control for adherence to NECA and SECA regulations uses an in-situ sensor, or sniffer, installed on a BN-2 Belgian Coast guard aircraft. The aircraft traverses a ship's exhaust plume to sample its emissions. As this is a costly and resource-intensive method, only a limited number of ships can be evaluated: ±10 ships per flight, with maximally 70 flights per year (Van Roy et al., 2022; Van Roy et al., 2022; Mellqvist and Conde, 2021). Placed near a crowded ship route, with approximately 20 to 30 ships per day, a remote sensing instrument can provide an additional and more permanent monitoring. However, as only a single route can be targeted, any new set-up should be complementary to the sniffer measurements, which are more spatially distributed. Moreover, remote sensing instruments show higher uncertainties than sniffers, and exhaust-based measurement techniques tend to underestimate emission factors, as it remains challenging to capture the core region of the plume (Beecken et al., 2023; Balzani Lööv et al., 2014). Therefore, the remote sensing system should function as an early warning system, enabling ships to be flagged for potentially high emissions and subjected to further inspections through other methods.

This work presents the Ship Emission Monitoring using Passive Absorption Spectroscopy (SEMPAS) instrument, with the objective to be sensitive enough to monitor the adherence to NO_x and SO_x emission regulations from individual ships in the North Sea, continuously and from a distance, based on the Differential Optical Absorption Spectroscopy (DOAS) technique. This remote sensing instrument measures NO_2 and SO_2 in the UltraViolet (UV) spectral range. Depending on visibility, the sensitivity to these gases extends up to ±10-20 km distance. This visibility is influenced by clouds and aerosols, the latter having a stronger impact in the UV than in the visible spectral range. Under actual observation conditions, the visibility can be estimated based on O_4 measurements following the method described by Wagner et al. (2004).

The DOAS technique quantifies atmospheric trace gas concentrations optically in the UV and visible ranges of the electromagnetic spectrum. NO_2 and SO_2 absorption strengths in this spectral region can be used as proxies for NO_x and SO_x emission factors (Hakkarainen et al., 2024; Alföldy et al., 2013). The ratio of SO_2 in SO_x emissions is constant, while NO_x is first emitted as NO and oxidised by ozone to NO_2. The NO_2 to NO_x ratio depends on plume dynamics and the local atmospheric O_3 content, thereby contributing to the uncertainty in the derivation of emission factors from trace gases observed in the UV by remote sensing.

The DOAS technique used in ground-based instruments has proven to effectively detect shipping emissions, with applications mainly concentrated in ports and inland waterways. Seyler et al. (2017) measured NO_2 and SO_2 with a Multi-Axis DOAS (MAX-DOAS) in the German Bight, with a similar set-up as this project. Krause et al. (2021) used a long-path DOAS to

https://doi.org/10.5194/egusphere-2026-3783
Preprint. Discussion started: 20 August 2026

measure NO_2 and SO_2 from individual ships in the Elbe river. A long-path DOAS has a retro-reflector, in this case across the river, limiting the lightpath to only contain the region of interest. Cheng et al. (2019) employed a MAX-DOAS configuration to measure ships in the portal areas of Shanghai and Shenzhen. Furthermore, the DOAS principle has also been used for shipping emissions studies in airborne applications: Berg et al. (2012) studied the feasibility of quantifying emission rates from airborne DOAS measurements. Emissions from single ships can also be seen from space under specific conditions, e.g. in NO_2 maps of the Sentinel 5-P TROPOMI instrument (Riess, 2024). As regulations have become increasingly stringent, the sensitivity of these instruments might become insufficient. Previous DOAS applications have not targeted cruising vessels in the open sea. The SEMPAS instrument aspires to address these limitations. In addition, SEMPAS provides insights in plume dynamics, through the introduction of imaging capabilities and the novel concept of actively tracking ships along their trajectory to acquire multiple measurements of the same vessel.

SEMPAS has been deployed in the context of several campaigns: First, at the third Cabauw Intercomparison for Nitrogen Dioxide Instruments (CINDI-3) campaign at the KNMI CESAR research site in the Netherlands, where it was tested next to other MAX-DOAS and imaging instruments. Secondly, on-shore at the port of Zeebrugge, Belgium, where it tracked ships on their way to the port of Antwerp. In the future, it will be installed off-shore on a transformer platform of a wind turbine park, 40km outside of the Belgian coast. From here, one of the highest-traffic ship routes of the North Sea, between 8 and 14km from the instrument's location, can be targetted. Ships detected by SEMPAS with high emission factors or FSC, will be flagged for more targeted fuel control.

Additionally, SEMPAS offers an opportunity for atmospheric trace gas research. SEMPAS can be used as conventional MAX-DOAS system acquiring atmospheric scans for trace gas identification. Previous marine MAX-DOAS measurements have been limited to shipborne campaigns (Schreier et al., 2015; Tan et al., 2018; Wang et al., 2020), or coastal instruments (Carpenter et al., 2010). A long-term MAX-DOAS instrument deployed at a fixed location in an entirely marine environment is thus unique, as such environments are difficult to access. The marine environment is underrepresented in satellite validation, highlighting the SEMPAS potential to contribute to validation activities. To combine the applications of ship emission and atmospheric monitoring using the MAX-DOAS technique, time is allocated dynamically: when a ship is within the field of view, the instrument tracks the vessel and conducts emission measurements; in the absence of nearby ships, the system operates in MAX-DOAS mode and conducts atmospheric scans.

2 Instrument Description

2.1 Instrumental components of SEMPAS

Using scattered sunlight, SEMPAS identifies atmospheric trace gases at distances up to ±10-20 km distance. In an automated measurement sequence, the instrument points towards the target scene, e.g. a ship's plume. This measurement principle is schematically depicted in Fig. 1. From the observed spectra, NO_2, SO_2 and other trace gas differential slant column densities (dSCDs) can be retrieved according to Sec. 3.

https://doi.org/10.5194/egusphere-2026-3783
Preprint. Discussion started: 20 August 2026

The core of the instrument is an Isoplane 160 grating spectrometer (Princeton Instruments, New Jersey). By placing the optics closely together and limiting the lightpath length and asymmetry, this spectrometer is optimised for imaging applications. It is equipped with a grating turret allowing for multiple gratings. Currently installed are a UV grating (295-395 nm, 0.4 nm Full-Width Half-Maximum (FWHM)) and a UV-vis grating (295-505 nm, 0.8 nm FWHM). To optimise the sensitivity to SO_2, a high spectral resolution is required. Also the detection of HCHO (another atmospheric gas of interest) is favored by using a high spectral resolution. Therefore the UV grating is preferentially used, both when measuring ships and in MAX-DOAS mode. This allows measurements of the SO_2 background and relate the shipping measurements directly to atmospheric variability. When deriving emission factors, the SO_2 and NO_2 observations are directly compared through their ratio. Accurate comparison requires both species to be measured within equivalent air masses. To this end, NO_2 from shipping emissions is also measured in the UV, ensuring a comparable light path for both gases. For other types of measurements the UV-vis grating could be used to measure NO_2 in the visible range, with better visibility and stronger absorption.

The detector is a 2048x512 pixels back-illuminated PIXIS 2D Charge-Coupled Device (CCD), cooled to -50 °C (Princeton Instruments). A filter wheel (Princeton Instruments) is placed at the entrance of the spectrometer, with multiple filters to reduce straylight. The UV grating uses a U340 filter, a bandpass filter with 340 nm center wavelength, and a FWHM of 85 nm. For the UV-vis grating a BG3 filter is placed, having a cut-off wavelength of 500 nm (while transmission starts again around 700 nm).

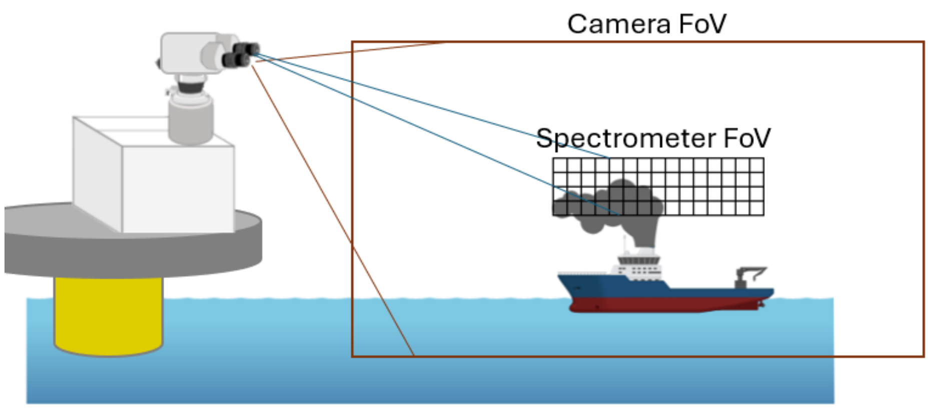

Figure 1. The general concept of SEMPAS: The target scene is registered as an image, by both the spectrometer and a conventional camera in the visible wavelength range. The shown field-of-views (FoV) of both channels are indicative. This camera and UV optics are mounted on top of the instrument in a rotatable optical head. A weatherproof box contains the spectrometer and electronics. The remote sensing instrument identifies ship emissions at distances of several kilometres from its installation location.

Light is fed into the spectrometer by an optic fiber bundle (Fiberguide Industries, New Jersey), with monofibers organised in a matrix. This allows the measurements to create a coarse resolution “image” of the observed scene, explained in Sec. 3.3. A focusing lens and the fiber bundle are mounted in the optical head, which can be rotated to orient the instrument toward the desired viewing direction. The optical head is moved by a pan-tilt system (Triyosys, Ankara), operating in the range of

https://doi.org/10.5194/egusphere-2026-3783
Preprint. Discussion started: 20 August 2026

-90 to 90° azimuth and -10 to 90° elevation. Accompanying the lens and fiber, the optical head houses a Prosilica GT 1290 camera (Allied Vision, Stadtroda), looking colinearly with the fiber at a field-of-view of 11 by 8.5°. This camera is used for ship identification and tracking. Lastly, Automatic Identification System (AIS) and Global Positioning System (GPS) receivers (Comar Systems, Newport) are mounted on the instrument, to localise and gain accurate information on ships in its area. Vessels are obliged to regularly transmit their position, course and ship information through the AIS system.

The measurement chain is automated through an internal fanless industrial computer (Neomore, Paris). It controls the instrumental components, climatology system, power supply and auxiliary electronic systems, and hosts the acquisition software and camera feedback loops. A router can provide internet connection over an ethernet cable or a 4G antenna. Data is transferred daily to BIRA-IASB servers, where it is processed further.

2.2 Spectrometer characterisation

The signal recorded by the detector pixels must be attributed to its respective sources, and the influence of contributions other than the signal of interest must be characterized. The following calibrations are applied: pixels-to-wavelength mapping, pixels-to-fibers mapping, dark current, electronic offset and straylight. The wavelength mapping on the pixels is twofold. First, a coarse alignment is carried out based on a HgCd-lamp, which exhibits sharp emission lines at fixed wavelengths in the UV. These known wavelengths can be assigned to a corresponding spectral pixel, and subsequently interpolated across the entire pixel-space. The second step is integrated in the DOAS retrieval (Sec. 3.1), and refines the alignment based on the solar atlas of Fraunhofer lines (Chance and Kurucz, 2010). This reaches an accuracy of a few picometers in wavelength alignment, necessary to identify the differential structures in the spectrum's optical density. The intensity over the spatial dimension of the detector shows a pattern of pronounced peaks, systematically spaced. These correspond to the positions of individual fibers, allowing them to be distinguished in the detector space. The mapping principles are visualised in Fig. 2. Dark current - charges on the CCD arising from thermal energy - is essentially non-existing in this detector, as it is cooled to -50 °C. Nevertheless a dark current measurement series is established every night, by recording measurements at various integration times in the absence of light. This can be used in case of instabilities in the detector temperature. The electronic offset - an artificial offset added to the CCD to ensure it always receives a positive signal - plays a more significant role due to its variability (around 600-650 counts). It is therefore measured before and after every MAX-DOAS scan or ship tracking sequence, by performing a 3 msec measurement (minimising the contribution of dark current) with a closed filter wheel. The alignment, both azimuth and elevation, between the camera and fiber bundle is calibrated based on a white line on a black surface, which can be observed accurately in intensity of the spectrometer as well as camera images.

Straylight characterisation is a complex aspect of calibration. Straylight refers to undesired light reaching the detector, originating either from external sources or from internal reflections within the spectrometer. It can manifest as either spatial or spectral straylight, depending on which dimension of the detector is affected. Spatial straylight is negligible compared to the variability in light distribution due to the fibers. Out-of-band spectral straylight, originating outside of the spectral range of interest, can be effectively blocked by a filter (Sec. 2.1). In-band spectral straylight, originating from and affecting the spectral range of interest, cannot be corrected optically. It is characterised in the lab and corrected for in post-processing. A

https://doi.org/10.5194/egusphere-2026-3783
Preprint. Discussion started: 20 August 2026

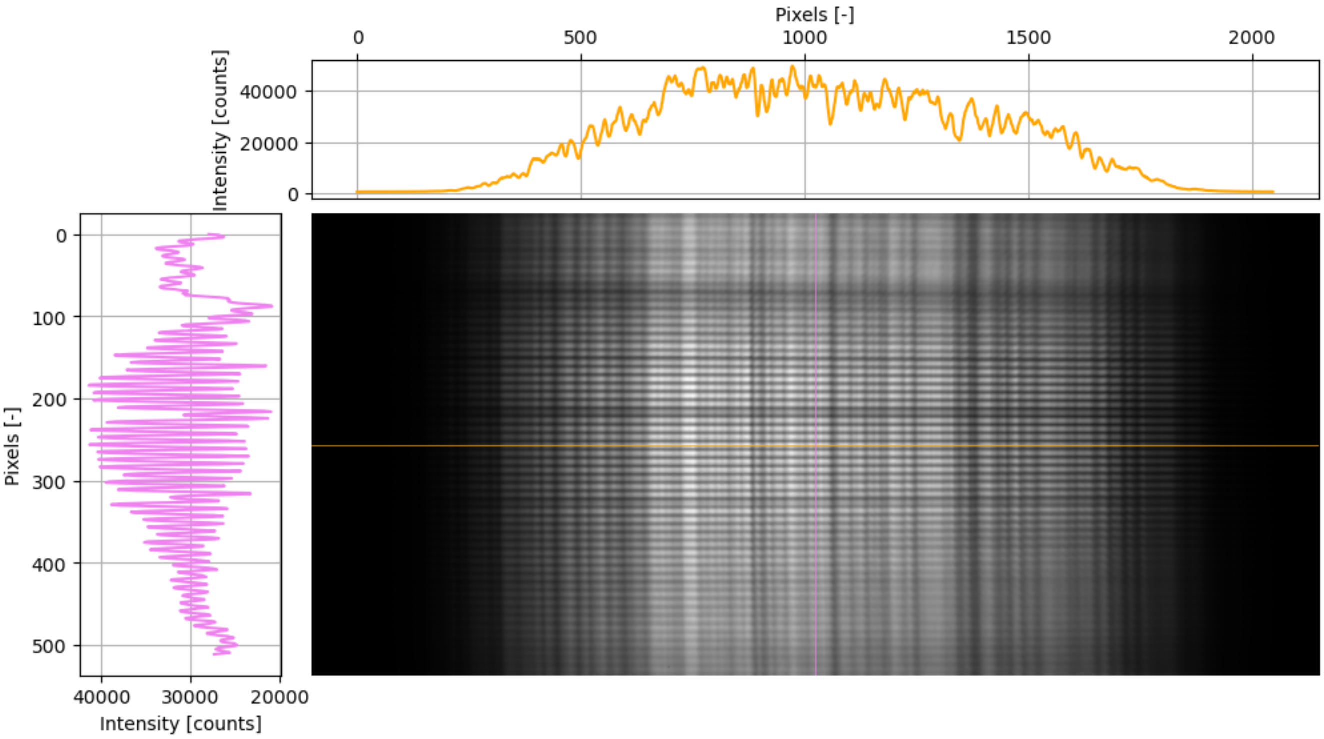

Figure 2. Direct intensity readout of a clear-sky measurement on the SEMPAS CCD. The horizontal axis shows the spectral dimension, with on top of the image a transect along the orange line. A typical atmospheric UV-spectrum from this instrument at a resolution of +-0.5nm is seen, with on the left the extinction by ozone absorption and on the right the cut-off by the U340 filter. The vertical axis shows the spatial dimension, with a transect on the left, where the peaks represent the light intensity caught by individual fibers, enabling to distinguish them.

line source is introduced at a certain wavelength and the extremities of the Gaussian line shape are analysed, following the method of Zong et al. (2006). Repeating this process at a range of wavelengths, the straylight behaviour over the spectral range is characterised. For the SEMPAS system, this was done with the double Bentham monochromator from the Belgian Radiometric Characterization Laboratory (B.RCLab, https://brclab.aeronomie.be/laboratory/wavelength-scale-calibration) at BIRA-IASB, for both gratings.

2.3 Robust housing for marine environment

The marine environment is characterized by large temperature variations, strong winds and persistent sea spray, resulting in humid and saline conditions that are harsh for material durability. To protect the optics and electronics, the instrument has a robust housing, which was designed and built in-house. Figure 3 shows this housing with instrumental components indicated. The box structure of welded stainless steel with double rubber seals protects the instrument from rain and moisture. Outside surfaces are surface treated and covered with a corrosion-mitigating paint. The instrument, additional components and power

https://doi.org/10.5194/egusphere-2026-3783
Preprint. Discussion started: 20 August 2026

system are entirely deployed inside this box, to limit cables going to the outside. The cable connectors are waterproof, IP68 rated. The optical window is cleaned manually on a monthly basis.

A closed-loop climatology system makes sure the temperature of the optics is stabilised to 28±0.3 °C. To overcome external temperature fluctuations, a multiple-layer control strategy based on Peltier systems is employed. The detector and auxiliary electronics are enclosed within a thick layer of insulation and regulated by three 480 W Peltiers, to compensate for changes of the ambient environment and govern extreme environments. Inside this enclosure, a second insulation layer and an additional 70 W Peltier are placed directly around the spectrometer, to react to any temperature variations inside the larger housing.

The spectrometer experienced mechanical vibrations during operation, both from external sources, such as heavy machinery operating nearby, and internal, such as the fans of the Peltiers. To mitigate this, 6 mm rubber damping mats were installed underneath the spectrometer and beneath the housing. Ferrite-cores are attached to the cabling of the detector, as precautionary measure for electro-mechanical interferences. At the optical head, a baffle is installed to limit interferences from direct sunlight. The baffle is relatively large to ensure it remains outside the camera's field-of-view. The optical head in itself is also an airtight enclosure, however without active temperature control. A simple fan is incorporated to cool the camera, the only electronical component in this smaller box.

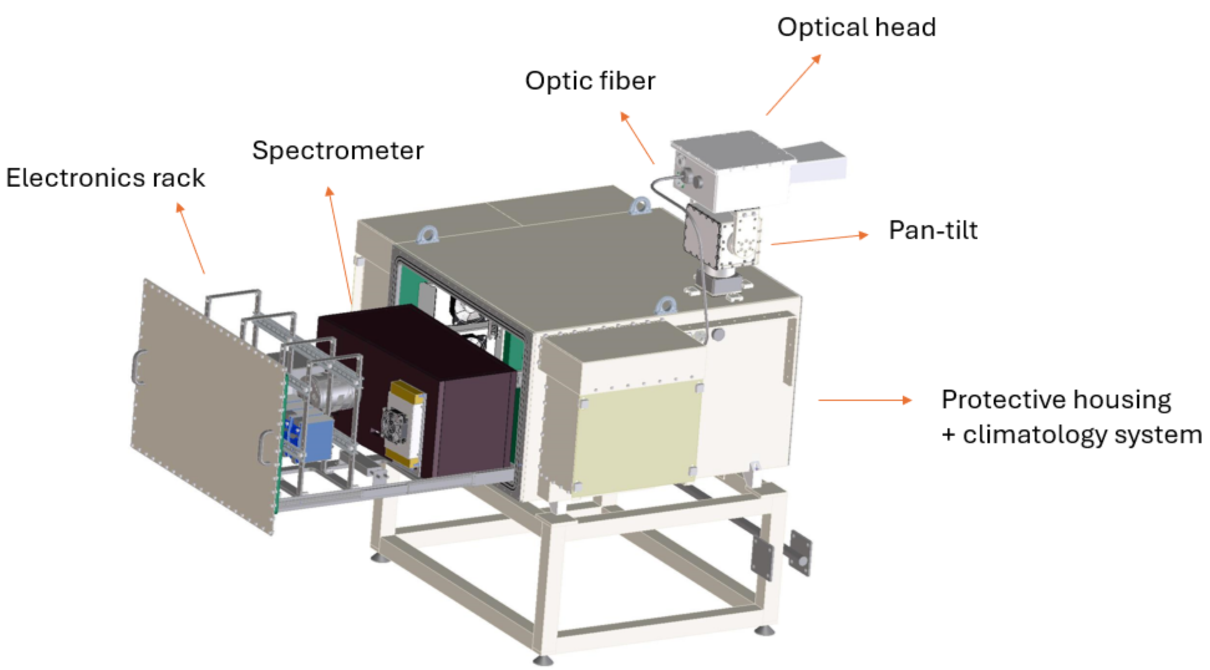

Figure 3. Design rendering of the SEMPAS housing. The image shows the mechanical implementation of the concept in Fig. 1, designed for withstanding the marine environment. Key components are indicated with arrows.

https://doi.org/10.5194/egusphere-2026-3783
Preprint. Discussion started: 20 August 2026

2.4 Ship tracking algorithms

To increase the number of measurements per ship plume, vessels are actively tracked along their trajectory using a dedicated algorithm. Initially, the approach involved averaging measurements acquired during tracking to enhance sensitivity. However, due to the turbulent nature of the plume and its temporal variability, the emission cannot be consistently captured. Consequently, multiple measurements obtained from one single ship are analysed separately.

The algorithm consists of two main components: AIS, to get ship information and location, and YOLO (You Only Look Once), open source image recognition software (Ultralytics, https://github.com/ultralytics/yolov5).

With an AIS and GPS antenna, ship locations are known within a certain range relative to the instrument's position. When a ship approaches the field-of-view, an alert is sent to the tracking software. The optical head points to the received location of the ship, awaiting the ship to enter the camera view.

The next processing block activates, the YOLO algorithm. YOLO is image recognition software, trained specifically for this application on a dataset of ship images at representative distances, contrast and background for a marine observation scene. The training distinguished between ships relevant for observation, such as tankers and container ships, and smaller ships not subjected, such as sailboats and fishing vessels. As the training required manual annotation, the dataset was limited to a few hundred images. Nonetheless the recognition performs well under a range of visibility and contrast conditions, as illustrated in Fig. 4. The confidence level of the recognition is indicated in green, and depends strongly on weather conditions and distance of the ship relative to the instrument. The size and colour of the ship have little influence on the performance. Confidence levels of 0.25 and above are accepted as valid recognitions. To represent the contrast of the ship on the image, an uncertainty value of the ship recognition is configured based on this confidence level, the number of missed detections in consecutive images, and the variability in detected size of the same ship. During operations, every recognition saves the annotated image and its label. The training dataset can hence be expanded with representative data, and the model can be retrained to improve its own performance.

Based on two consecutive recognitions of one ship, the vessel angular velocity relative to the observer location is estimated. The optical head starts rotating at this speed. To guarantee continuous tracking without drift or jumps, a feedback loop is established based on the camera feed. By adjusting the speed, the ship is kept in the centre of the image. In this way, the instrument accurately follows a ship along its trajectory.

https://doi.org/10.5194/egusphere-2026-3783
Preprint. Discussion started: 20 August 2026

Figure 4. The YOLO image recognition software is trained on a database of ship images. The green box indicates where the algorithm recognises a ship and denotes the confidence level of the recognition. It recognises ships in various conditions, at large distance and low contrast.

The feedback loop consists of a PID-regulator (Proportional-Integral-Derivative). It controls parameters in a dynamic system based on the deviation from their desired value. The PID-loop adjusts the tracking speed, based on the deviation from the centre of the ship in the image. To have a closed-loop system with all parameters defined, the velocity form of the PID equation is used:

$$v_n = v_{n-1} + K_p \cdot (e_n - e_{n-1}) + K_i \cdot e_n \cdot \Delta t + K_d \cdot \frac{e_n - 2e_{n-1} + e_{n-2}}{\Delta t} \tag{1}$$

With v the velocity, K_p, K_i, K_d the PID gains and e the error. n denotes the current measurement number, and Δt is the time difference between current and previous measurement. The algorithm operates in pan-tilt system coordinates. The loop is initiated by the speed estimate based on two consecutive images of the ship. The current rotation speed is then adjusted according to the feedback loop.

Multiple tracking checks are incorporated into the procedure. The algorithm detects situations involving multiple ships within view, including crossing or overtaking vessels, and consistently maintains tracking of the originally selected ship. Lastly, the aiming point of the spectrometer is adjusted for ship speed and heading, wind speed and direction. Generally, the stack is situated at the rear of the ship. To account for this, the aiming point is adjusted towards 3/4 of the width of the ship, oriented to the rear. Furthermore, the wind and ship velocity vectors, obtained from local meteorological stations and AIS information respectively, are projected onto the measurement plane, into an apparent wind vector. The aiming point is relocated along this apparent wind vector, downstream of the plume, by 0.01% of the vector (defined manually based on relative ship size at a typical distance of 8km) on the native pixel grid of the camera image. Aiming downstream of the stack allows for a stronger NO_2 signal, after its conversion from the emitted NO. Plume dispersion, wind conditions and accuracy of the tracking

https://doi.org/10.5194/egusphere-2026-3783
Preprint. Discussion started: 20 August 2026

algorithm influence the optimal aiming point for intercepting the plume. This can be progressively refined based on experience of ships observed at the installation site.

The estimated tracking time per ship while crossing the azimuthal field-of-view of the instrument was approximately 10 minutes during the test period in Zeebrugge, and will increase to 30 minutes for the future installation on the off-shore wind park platform. This depends on visibility and contrast of the recognition, and disturbing factors, such as crossing ships or wind turbines in the field-of-view. Following manual tuning, the K_p, K_i and K_d gains of the regulator are set to 0.2, 0.01 and 0 respectively. The average tracking error is ±10 pixels, or 0.05°. An oscillation remains in the control response of the system, originating from the time delay between registering the image and adjusting the speed. The delay is dominated by the communication to and activation of the new speed in the pan-tilt system. The oscillation has a period of 25 s and an amplitude of 10 pixels. The width of the fiber bundle spans 250 pixels, while one fiber is approximately 17 pixels wide. The oscillation and tracking error fall in the field-of-view of the instrument, limiting the effect on the measurements.

3 Retrieval methods

3.1 Differential Optical Absorption Spectroscopy (DOAS)

The DOAS method, following Platt and Stutz (2008), allows to retrieve atmospheric pollutants from remote sensing measurements. Light fed through a spectrometer is spectrally analysed for fingerprints of certain trace gases. Optical absorption spectroscopy measures the attenuation of the light spectrum through an absorbing medium. This attenuation can be described by the general Lambert-Beer law, for the absorption of electromagnetic radiation through a gaseous medium:

$$I(s,\lambda) = I_0(\lambda) \cdot exp[-\int_s^0 n(s') \cdot \sigma(\lambda, T(s'), p(s'))ds'] \quad (2)$$

The equation shows the intensity after absorption as a function of wavelength λ with:

- I_0 the intensity of radiation entering the medium
- n the number density
- σ the absorption cross-section of an absorbing species
- T the temperature calculated along lightpath s
- p the pressure calculated along lightpath s
- s the line of sight

Passive absorption spectroscopy methods use sunlight as a source. SEMPAS is based on the MAX-DOAS technique, utilising scattered sunlight by observing the sky at multiple viewing angles. The absorbing gases and scattering particles in our atmosphere interact with this sunlight through Rayleigh and Mie scattering along the observed lightpath, complicating the application of this concept. Therefore, a differential approach is taken: the measured spectrum is logarithmically compared to

https://doi.org/10.5194/egusphere-2026-3783
Preprint. Discussion started: 20 August 2026

a reference spectrum, and the resulting differential optical density is studied for the presence of absorptions of trace gases. This approach eliminates factors such as the absorption from the solar atmosphere or instrumental properties. The reference spectrum used in SEMPAS is a zenith measurement, taken either daily at noon or before and after every measurement sequence. By comparing the off-axis measurements to this reference, the stratospheric component is eliminated and a tropospheric column can be determined. The residual of the measured spectrum is fit for cross-sections of expected gases within a certain spectral range. A pseudo cross-section is added to account for the Ring effect, coming from Raman scattering of air molecules. The cross-sections are laboratory-measured for a representative temperature and pressure. The fitting retrieval uses the linearised DOAS equation:

$$\ln(\frac{I(\lambda)}{I_0(\lambda)}) = -\sum_{i=1}^{N} S_i \cdot \sigma_i'(\lambda) - \sum_{p} c_p \cdot \lambda^p + r(\lambda) \quad (3)$$

The integrated number densities in molec/cm^2 or differential Slant Column Density (dSCD) are retrieved for a certain trace gas, along the lightpath s:

$$S_i = \int n_i(s) ds \quad (4)$$

Along with the cross-sections of these trace-gases, a polynomial is fit to partly account for scattering and broad-band structures, described by coefficients c_p. The remaining residual after the complete fitting procedure is $r(\lambda)$, representing the noise in the measurement. The retrieval algorithm is implemented in the QDOAS software (Danckaert et al., 2017), developed at BIRA-IASB.

For shipping emission measurements, the viewing angle is limited to angles directly above the ship, close to the horizon. In the so-called MAX-DOAS mode of the instrument, a scan of the atmosphere is acquired by a fixed sequence of viewing angles adopted from Kreher et al. (2020). The main objective of SEMPAS is to measure ship emissions, based on a background measurement outside of the ship plume, and a measurement through the ship plume. Both are analysed with respect to the same zenith reference, taken closely in time. The dSCDs inside the plume and the background can be compared to quantify the enhancement due to the emission of the observed ship.

3.2 MAX-DOAS mode for atmospheric trace gas measurements

Marine environments are of particular interest for atmospheric trace gas measurements, given the absence of permanent MAX-DOAS measurements at offshore locations. In the absence of nearby ships, SEMPAS hence functions as a conventional MAX-DOAS instrument performing atmospheric scans. In MAX-DOAS mode, the intensities from all fibers are binned, to obtain a high signal-to-noise ratio and sensitivity. Incorporating this measurement mode required no instrumental modifications, and allows periods without ships to be effectively exploited. Furthermore, the Fiducial Reference Measurement for DOAS instruments (FRM4DOAS) framework (Van Roozendael et al., 2024) can be used for data processing. Among other products, tropospheric Vertical Column Densities (VCD's) and tropospheric vertical profiles of NO_2 and HCHO are computed using

https://doi.org/10.5194/egusphere-2026-3783
Preprint. Discussion started: 20 August 2026

dSCDs towards multiple low and intermediate elevation angles for profile inversion (Hönninger et al., 2004; Wittrock et al., 2004). While the FRM4DOAS framework comprises two tropospheric profiling algorithms, the Mainz Profile Algorithm (MAPA) (Beirle et al., 2019) and Mexican MAX-DOAS Fit (MMF) (Friedrich et al., 2019), only the results of the latter are delivered as final products while the former serves as a quality control. Both algorithms ingest, apart from the dSCD of the trace gas in question, dSCDs of the oxygen collision-induced complex O_4 to estimate the aerosol profile needed for the trace gas retrieval. The framework accounts for the air mass at the time and geometry of measurement, to cancel the observation's dependency on atmospheric lightpath. VCDs then provide a physically representative baseline for analysis of the results and comparison to other measurements.

Depending on maintenance cost, the instrument aims at an operation of minimally one year, to study the variability of trace gases across different time scales. A timeseries of measurements in various meteorological conditions, both atmospheric scans and shipping emissions, would give an idea of the marine background concentrations, transported coastal emissions and local perturbations. The atmospheric measurements can also be used for satellite validation, for example of the Sentinel-5P TROPOMI instrument or future similar missions.

3.3 Imaging DOAS principle

The light-collecting fibers are arranged in matrix configuration, where each monofiber acts as a discrete sampling element corresponding to a pixel. Combining these pixels, a coarse image of the observation scene is constructed, as shown in Fig. 1. The size of the image is limited by the size of the detector, which captures 55 fibers, corresponding to a matrix with a top row of 11 fibers, two middle rows of 15 fibers, and a bottom of 14 fibers. The entrance of the fiber is equipped with a telelens of focal length 78 mm. This creates a field of view of 1.4 by 0.38°, or 260 by 66 m at 10 km distance. This comprises 15 by 4 pixels, with the field of view per pixel 0.14° or 24 m diameter, not taking overlap into account.

Following spectral analysis, this image is converted to an NO_2 or SO_2 dSCD picture, enabling the spatial visualization of complex plume structures. Variations in the NO_2 field facilitate the distinction between pixels located inside the plume and those representing background conditions. The plume location relative to the ship depends on wind conditions, plume dispersion and ship speed. While wind and ship vectors are accurately known through an on-site meteorological station and AIS information, plume dispersion remains difficult to constrain. An instantaneous outlook of the plume is turbulent and challenging to model. Within a time series of images acquired during ship tracking, the motion of the plume can sometimes be identified. This improves the delineation between plume and background regions and supports a more accurate estimation of ship emissions.

The slit formed by the vertical arrangement of the 55 fibers is projected onto the 2048x512 pixel detector. To match the spatial extent of the fibers, detector rows 14 to 509 are combined in bins of 9 rows, yielding an image corresponding to 55 fibers. The intensities binned per fiber are recomposed into the original matrix structure of the fiber bundle. The resulting image can suffer from inter-pixel variability artefacts, treated analogously to and further denoted as striping, arising from the variable response of the individual fibers (cfr. the spatial dimension of Fig. 2), as well as the binning procedure: although an integer number of detector rows is assigned per fiber, the fiber does not span an exact integer number of rows, leading to unequal light

https://doi.org/10.5194/egusphere-2026-3783
Preprint. Discussion started: 20 August 2026

distribution among bins. A destriping correction is applied to the data, in which deviations from a polynomial fit are determined for each fiber using the average of multiple clear-sky measurements, and subsequently subtracted from the retrieved NO_2 and SO_2 fields (Tack et al., 2017; Lawrence et al., 2015).

3.4 Fitting windows and spectral analysis

The spectral retrieval windows used in SEMPAS are consistent with those described in Kreher et al. (2020). An overview is given in Table 1. As a baseline for all measurements, the UV grating is used - to be able to identify SO_2 - and hence the UV window for NO_2. As mentioned, HCHO, another gaseous pollutant affecting air quality, can also be identified in the UV. If SO_2 retrieval is not required, the UV-vis grating can be used to increase sensitivity to NO_2. In the visible spectral range, the the higher light intensity improves the signal-to-noise ratio, reducing retrieval uncertainties. In addition, visible wavelengths are less affected by aerosol scattering than UV wavelengths, resulting in longer effective lightpaths and increased sensitivity to trace gases over larger distances. With the UV-vis grating, all three NO_2 windows can be used, with varying sensitivity to NO_2, however the SO_2 window cannot be reliably fitted due to insufficient light level at the shortest wavelengths covered by this grating. O_4 is identified in the corresponding NO_2 window. The SO_2 fitting window is a compromise between low intensity levels around 300 nm due to strong ozone absorption, and the decrease of absorption strength at higher wavelengths. Wang et al. (2014) proposes a window of 305-317 nm, which for SEMPAS is shortened to 308-317 nm to reduce noise, consistent with previous shipping emissions MAX-DOAS applications (Seyler et al., 2017).

https://doi.org/10.5194/egusphere-2026-3783
Preprint. Discussion started: 20 August 2026

Table 1. Properties of the various fitting windows used for SEMPAS.

Window name	NO_2 UV	NO_2 vis-small	NO_2 vis	SO_2	HCHO
Fitting range [nm]	338–370	411–445	425–490	308–317	324.5–359
Main species	NO_2, O_4	NO_2, O_4	NO_2, O_4	SO_2	HCHO
Cross-sections (K)	NO_2 (220, 294)[a]	NO_2 (220, 294)	NO_2 (220, 294)	NO_2 (294)	NO_2 (220, 294)
	O_4 (293)[b]	O_4 (293)	O_4 (223, 293)	O_3 (223, 243)	O_4 (293)
	O_3 (223, 243)[c]	O_3 (223)	O_3 (223)	HCHO (298)	O_3 (223, 243)
	HCHO (298)[d]	H_2O (293)	H_2O (293)[g]	SO_2 (298)[h]	HCHO (298)
	BrO (223K)[e]	Ring	Ring	Ring	BrO (223)
	Ring[f]				Ring
Polynomial degree	5	4	5	5	5
Intensity offset	Slope	Constant	Constant	Slope	Slope

[a] Vandaele et al. (1998)
[b] Finkenzeller and Volkamer (2022)
[c] Serdyuchenko et al. (2014)
[d] Meller and Moortgat (2000)
[e] Fleischmann et al. (2004)
[f] Chance and Kurucz (2010)
[g] Rothman et al. (2013)
[h] Vandaele et al. (2009)

The SEMPAS data considers two applications: binned data corresponding to the MAX-DOAS mode, and data binned per fiber for the imaging applications. Occupying the UV grating, the uncertainties on the retrieved slant columns as calculated based on the DOAS fit, typically are 5e14 for NO_2 and 1e15 for SO_2 in the binned case, and 2.3e15 for NO_2 and 4.4e15 for SO_2 in the imaging case. Figures 5 and 6 illustrate spectral fits in the UV fitting windows, both for the binned and imaging case. With 55 fibers, the maximum improvement of the residuals would be a factor $\sqrt{55}$ or 7.4, when going from binned per fiber to fully binned. In practice, the signal is not evenly distributed across the detector and multiple noise sources contribute.

https://doi.org/10.5194/egusphere-2026-3783
Preprint. Discussion started: 20 August 2026

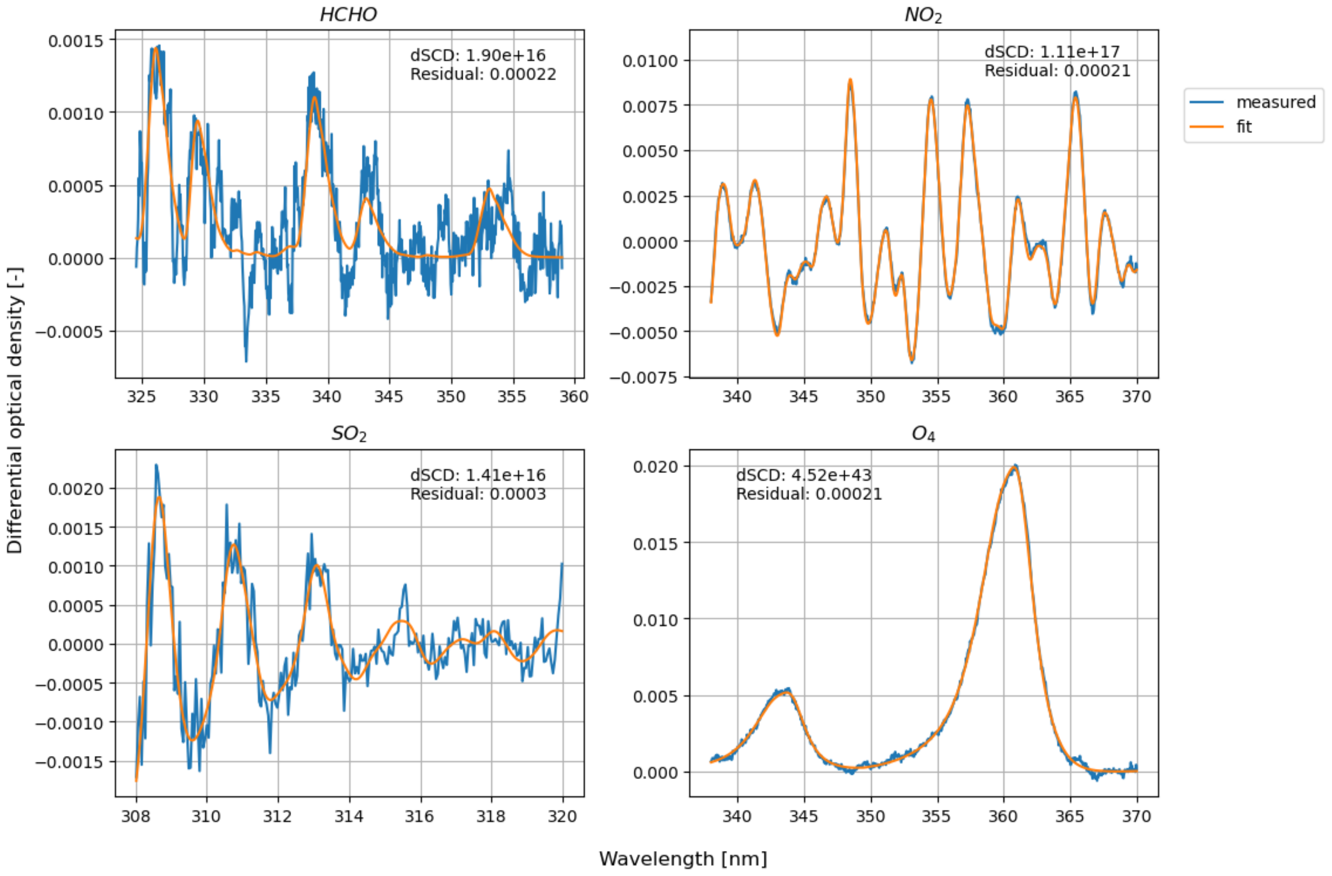

Figure 5. DOAS retrieval fits for the UV fitting window on binned data, for SEMPAS in Zeebrugge on 06/04/2025 14:54, at 58.67 solar zenith angle. The blue curve shows the normalised differential optical density of the measurement, while the orange curve shows the fitted cross-section for each trace-gas, with its fitted dSCD value and residual indicated.

https://doi.org/10.5194/egusphere-2026-3783
Preprint. Discussion started: 20 August 2026

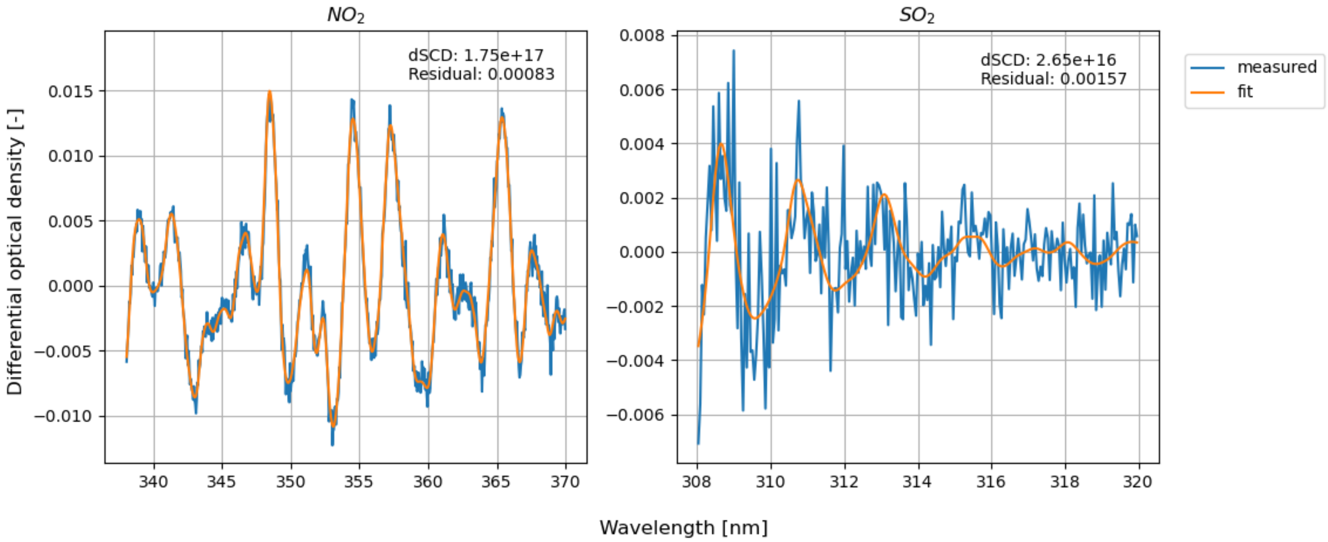

Figure 6. DOAS retrieval fits for the UV fitting window on data binned per fiber, for SEMPAS in Zeebrugge on 07/04/2025 14:04, at 52.28 solar zenith angle. The blue curve shows the normalised differential optical density of the measurement, while the orange curve shows the fitted cross-section for each trace-gas, with its fitted dSCD value and residual indicated. The data binned per fiber is used for ship tracking in imaging mode, for which only NO_2 and SO_2 are relevant.

4 Results of the participation to the CINDI-3 intercomparison campaign

During the CINDI-3 campaign in June 2024, MAX-DOAS instruments measuring NO_2 were co-located aside one another at the KNMI CESAR research facility, to intercompare the measured dSCDs (Kreher et al., in prep). Simultaneously, a range of auxiliary instruments were deployed, including in-situ sensors, sondes, lidar, mobile and airborne measurements. Over 40 instruments from international research groups participated, both established MAX-DOAS and research-grade instruments. The instruments followed a similar observation schedule and fixed retrieval settings to enable direct comparison. SEMPAS participated as a MAX-DOAS instrument to benchmark its performance against established NO_2 instruments. To this end, NO_2 and O_4 were retrieved using the UV-vis grating to assess the maximum achievable sensitivity. Its imaging capabilities were also tested, to assess the resolution and homogeneity of the generated images. During this campaign the fiber matrix was exchanged for a horizontal line bundle of 51 monofibers, covering a field-of-view of 7.65 by 0.15°. An image was acquired as a push-broom scan, combining measurements at incrementally increasing elevation angles. Using a step size of 0.2°, an image of 7.65 by 4° could be constructed in 20 measurements of 30 s. Because of the variability in response of individual fibers, the push-broom imager exhibits row-dependent artefacts. A destriping correction is applied by subtracting the deviation of the average of measurements above 1.2° elevation angle, to avoid true NO_2 horizontal structures, from a 3^{rd}-degree polynomial.

SEMPAS collected data on 4 out of 18 campaign days, using all three NO_2 fitting windows described in Sec. 3.4, similar to 17 other 2D MAX-DOAS or equivalent instruments. The SEMPAS performance in the intercomparison framework is

https://doi.org/10.5194/egusphere-2026-3783
Preprint. Discussion started: 20 August 2026

evaluated relative to the median of all participating instruments (Friedrich et al., in prep). Figure 7 shows a comparison of one day of SEMPAS data to this campaign median, in the NO_2 VIS window using a daily noon reference. At higher dSCDs, SEMPAS underestimated the median results, while at lower dSCDs they were in good agreement. This likely originated from a mismatch in the instrument's elevation angle setting. The SEMPAS results are interpolated 0.25° downwards, giving an excellent agreement with the campaign median. A correlation of 1 is found, without slope or offset, and a root mean square (RMS) of 1.5e15, where the error is defined as the difference between data from SEMPAS and median data. The results demonstrate that the SEMPAS instrument, equipped with the UV–vis grating, achieves performance in the NO_2 VIS retrieval window comparable to that of established research-grade MAX-DOAS instruments. As the remaining instrumental characteristics are identical, these findings are expected to be representative for other configurations, such as the UV grating, as well.

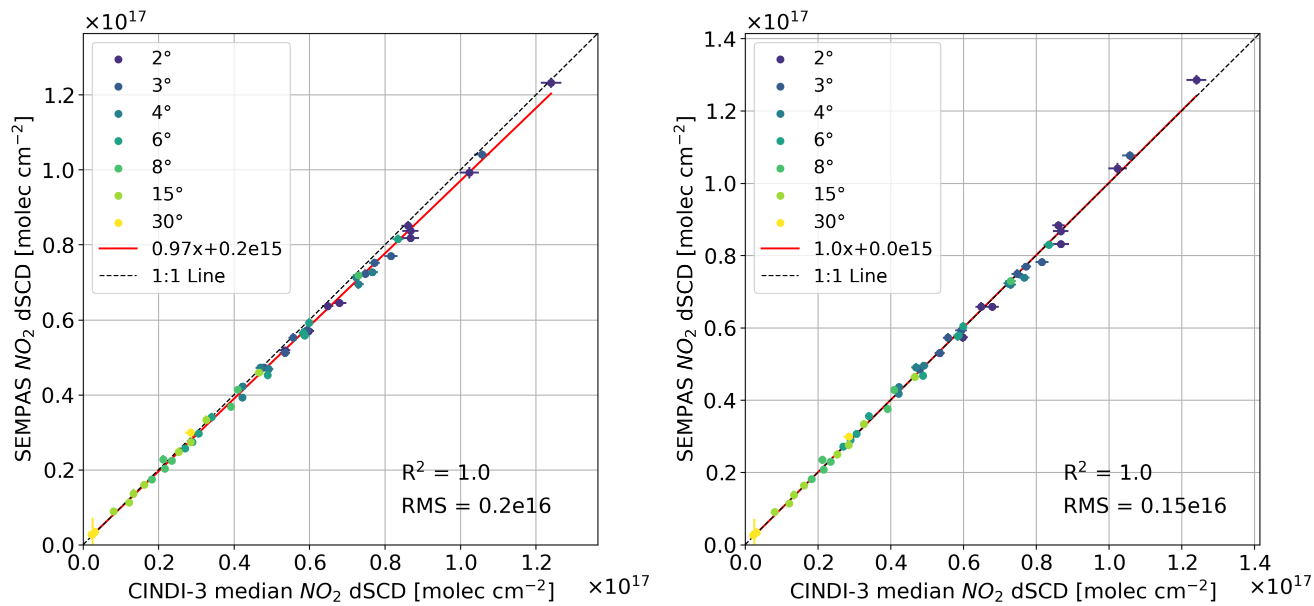

(a) No elevation misalignment correction

(b) -0.25° elevation misalignment correction

Figure 7. Correlation of SEMPAS MAX-DOAS measurements with the camapign median result of all participating MAX-DOAS instruments over various elevation angles, on the day of 17 June 2024 during the CINDI-3 campaign in June 2024 in Cabauw. The correlation plot shows error bars for SEMPAS as defined by the measurement uncertainty, while the error bars of the median data are given by the standard error of the instrument data. (a) Shows the original data comparison. (b) A SEMPAS upward elevation misalignment of 0.25° is taken into account by interpolating the measurements downward.

Two other imaging intruments participated in the campaign: IMPACT (Peters et al., 2019) and the NO_2 camera (Gramme et al., 2025). The three instruments operate in different ways and with varying field-of-views. During the campaign, they acquired images simultaneously, targeted at the Cabauw church to facilitate cross-referencing, located 2 km from the measurement

https://doi.org/10.5194/egusphere-2026-3783
Preprint. Discussion started: 20 August 2026

site. A detailed comparison is presented in Busschots, et al. in prep. Figure 8 illustrates the imaging capabilities of the SEMPAS instrument.

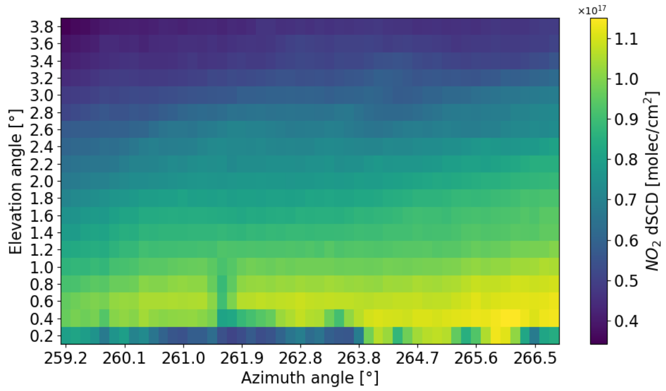

Figure 8. Example of an image of the NO_2 field around the Cabauw church measured by SEMPAS, taken at 17 June 2024 12:55 during the CINDI-3 campaign. An image is created by performing a vertical scan of a horizontal 7.65 degree fiber bundle in steps of 0.2 degrees.

To reduce out-of-band straylight, the use of a BG3 band-pass filter proved challenging during CINDI-3. The filter wheel is placed between the fiber bundle and the slit of the spectrometer, in the optical path where the fibers are matched to the slit. Inserting a filter alters the optical path, degrading the instrumental resolution and fitting results. Consequently, the out-of-band straylight was reduced in post-processing. Below 300 nm, strong ozone absorption prevents any light reaching the detector; an observed signal in this range is considered straylight. Its value, $\pm 5\%$ of the maximum intensity, can be quantified and subtracted from the measurement as a constant spectrum. To account for spectral structures of the straylight, an alternative approach involves a spectrum measured by a filter blocking UV and visible light, capturing only the out-of-band straylight. Scaled by the constant straylight value, the resulting spectrum can be subtracted from the measurements. In practice, negligible differences were observed between these methods. A constant spectrum was applied to the CINDI-3 measurements, to avoid introducing additional errors from a manually measured spectrum. This correction reduces the straylight, but residual straylight can still introduce a slant-column dependent bias, and therefore contribute to the slope observed in Fig. 7. After the campaign, the optical alignment of the instrument was adjusted with a filter in the optical path, restoring the resolution of the instrument and reducing out-of-band straylight to less than 0.05%.

5 Results of the installation in the sea port of Zeebrugge, Belgium

The instrument has been installed in the port of Zeebrugge, next to the traffic control tower of the Schelderadarketen on the Westerdam (Fig. 9 and 10) from 13 March until 12 May 2025. From here, it points in between the breakwaters at the port entrance, monitoring the shipping lane in the direction of the port of Antwerp. SEMPAS does not target ships entering the port of Zeebrugge itself, as these are too close and cannot be recognised and pointed to by the ship tracking algorithm. The

https://doi.org/10.5194/egusphere-2026-3783
Preprint. Discussion started: 20 August 2026

measurement principle is as follows: by default, the system performs atmospheric measurements in the form of MAX-DOAS scans. When an AIS signal indicates a ship approaching the field of view, background measurements are conducted at the target azimuth where the ship is expected to appear. The ship is tracked until it leaves the measurement range, after which additional background measurements are performed. This operation is bracketed by zenith measurements for sequential referencing of the DOAS observations.

Figure 9. Situation of the port of Zeebrugge on the Belgian coast in panel (a), with the instrument installation location and field of view indicated in the zoomed image in panel (b). Map © OpenStreetMap contributors, satellite image Landsat / Copernicus © 2025 Airbus.

https://doi.org/10.5194/egusphere-2026-3783
Preprint. Discussion started: 20 August 2026

Figure 10. SEMPAS installed in the port of Zeebrugge. It observes through the gap between the breakwaters to ships passing in a distance, going towards or coming from the port of Antwerp.

5.1 Shipping measurements

5.1.1 Tracking algorithm

During the installation in Zeebrugge, the ship tracking algorithm was further developed and for the first time tested on actual ships. The campaign served to experiment with the algorithm and benchmark its performance and robustness. Figure 11 illustrates the result of a tracking. The top left panel shows an image of the ship, taken every two seconds and processed to adjust the rotational speed of the instrument (Sec. 2.4). The top right panel shows the position of the tracker, in rotational steps, over the time of tracking. Over time the relative steps become smaller, denoting the ship moves further from the instrument. This is confirmed by AIS information. With increasing distance, the YOLO software encounters difficulties recognising the ship, leading to instabilities. Eventually the tracking process is terminated by a lack of consecutive recognitions over a period of time. The bottom left panel shows the tracking error, defined as the ship's position on the image defined by the YOLO

https://doi.org/10.5194/egusphere-2026-3783
Preprint. Discussion started: 20 August 2026

recognition, w.r.t. the aiming point. After processing by the PID-regulator, this tracking error yields the tracker rotational speed in the bottom right panel. At the start of tracking, the system requires an adjustment period to determine the appropriate rotational speed, after which it stabilises to a constant rate. An oscillation in the speed response (Sec. 2.4) is observed, with an amplitude remaining within the field-of-view of the instrument.

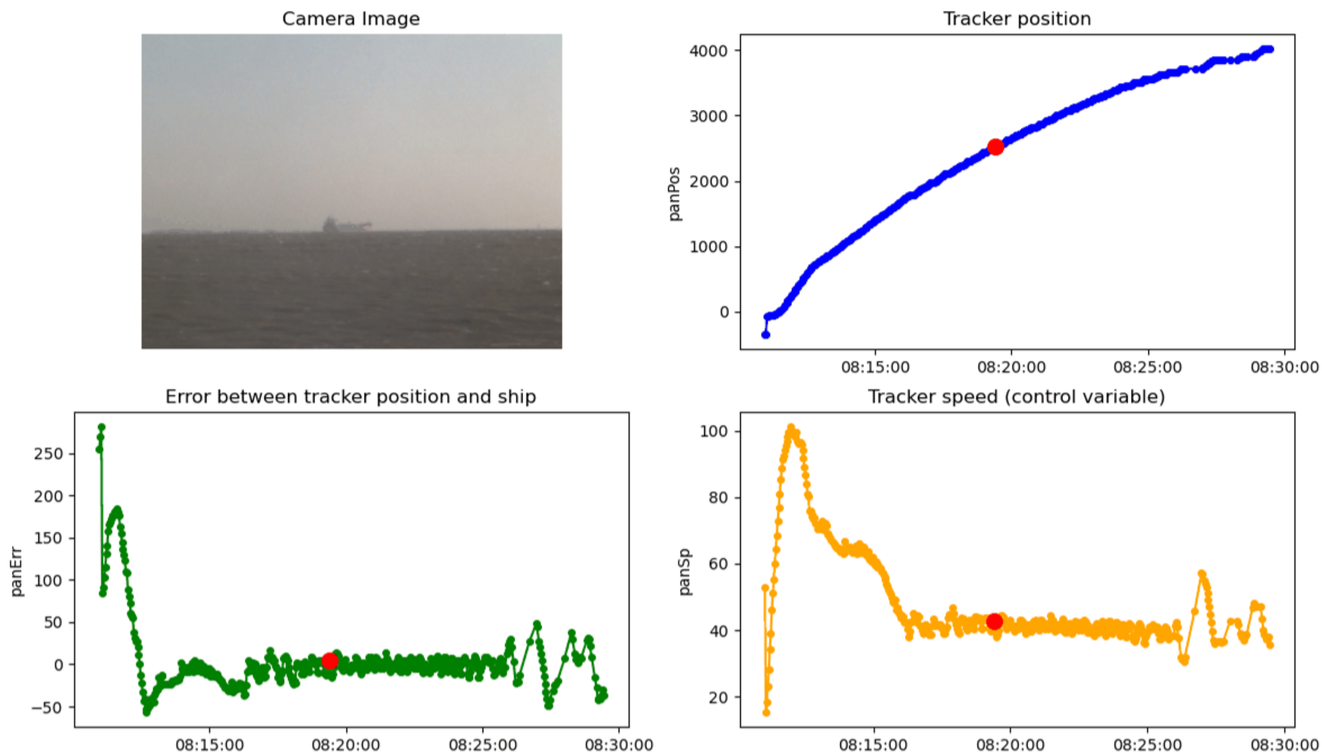

Figure 11. Results of the ship tracking algorithm, in rotational step coordinates of the pan-tilt unit. The image shown is taken at the time of the red dot indicated in the plots, in this case 06 May 2025 08:19:24. The full video can be found in the supplementary material.

5.1.2 Observations

Based on the information gained from tracking, measurements can be attributed to a certain ship. During the two-month campaign, a total of 501 ships were detected by the YOLO algorithm, typically between 10 and 35 per day at a distance between 7 and 11 km of the instrument. On 11 May 2025 a sailing event caused numerous sailboats to pass the camera. Observed closely to each other, the software can interpret the scene as one larger ship. The Zeebrugge campaign served as development phase for the tracking algorithm, during which unsuccessful trackings were needed to optimise the algorithm, configure the PID-parameters and refine the robustness of the tracking when multiple ships are in view. In 98 ship plumes, signals of both NO_2 and SO_2 were measured. Figure 12 presents statistics from the final week of the campaign, providing an indication of the performance of the operational system.

https://doi.org/10.5194/egusphere-2026-3783
Preprint. Discussion started: 20 August 2026

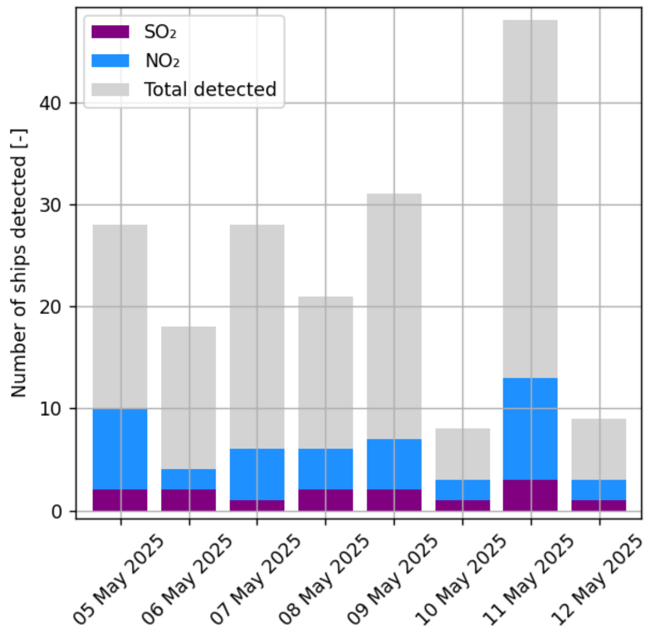

Figure 12. Number of ship detections by the YOLO software for the last week in Zeebrugge (05 to 12 May 2025), with indications of how many ship plumes are recognised in NO_2 and SO_2 measurements.

5.1.3 Case studies

With a stable tracking algorithm, measurements are acquired continuously at a fixed position relative to the ship. The total acquisition time is 1 minute, compromising between temporal resolution and signal-to-noise ratio. At constant emission rate and stable atmospheric conditions, a constant NO_2 and SO_2 value is expected throughout the tracking. Figure 13 illustrates various cases of typical observations, with the measurements averaged over the observed matrix. Purple points indicate periods of active ship tracking. Background measurements, shown in blue, are acquired prior to the ship entering the view and after the tracking ends (except if a measurement at 0.4° is available within 10 minutes before the tracking). The background measurements are taken in a scene when no ships are in view, but not necessarily without any emissions from other sources. No background corrections are applied to the measurements displayed in Figure 13. All measurements are taken at 0.4° elevation and filtered for RMS at a threshold of 0.001. Note the different scale per case, as the dSCD values show large variations (cfr. Sec. 5.2). In most cases NO_2 values exceed the background variability, but typically as a single peak instead of a constant signal throughout the tracking. This variability indicates a more dynamic scene than anticipated, influenced by factors such as fluctuating wind fields, inherent turbulence of the plume, varying NO-NO_2 conversion, and changes in measurement geometry w.r.t. the ship as the instrument continuously rotates in azimuth. SO_2 measurements exhibit higher uncertainties, but nevertheless peaks are observed in some cases. The SO_2 peak does not always occur simultaneously with the NO_2 peak, reflecting that SO_2 is emitted directly, while NO_2 is emitted as NO and oxidised later on. The sequence of the peaks

https://doi.org/10.5194/egusphere-2026-3783
Preprint. Discussion started: 20 August 2026

differs between cases: peaks may appear at the start of tracking, gradually build up, or even occur while the tracking algorithm is being initialized and the aiming point is not yet established (first case in Fig. 13).

Figure 14 shows a subset of individual measurements from one tracking (case 4 in Fig. 13) of a ship passing from left to right, visualising the entire spectrometer measurement matrix overlaid on the camera image. The dSCDs are destriped, based on the deviation from a polynomial fit through the fiber-based average of all measurements of that ship. The data is filtered for RMS, at a threshold of 0.005, and recomposed into the original matrix of the fiber bundle. The wind field is available in real time at an interval of 10 minutes, from the RMI Zeebrugge meteorological station. The wind vector, together with the speed vector of the ship, is projected onto the measurement plane. The aiming point for ship tracking is adjusted downstream, for the emitted NO to have been converted to NO_2 at the observation point. In Fig. 14 this shows as the measurement being taken in front of and above the ship. In many cases, only low values for SO_2 were observed, hence future applications should prioritise to aim as close to the stack as possible, optimising for the point in the plume with the highest SO_2 concentrations.

The ship tracking algorithm was stable throughout the tracking of Fig. 14, as the measurement point relative to the ship is constant. Only after several minutes into the tracking, an NO_2 signal from the plume emerges in the measured matrix, appearing smooth and clearly structured. Note that one measurement is acquired during 1 minute, meaning the turbulence of the plume is averaged over this measurement period. The plume enters from the right, transects the field-of-view, and fades toward the left. The latter can possibly be explained by the increasing distance between the ship and the instrument. The temporally irregular appearance of the plume can be attributed to the dynamic nature of the scene. In other cases, the observed peaks might not exceed the general background variations, although a local peak is observed (last case in Fig. 13). For SO_2, the plume structure is generally not visible in the matrix, leaving the attribution of enhancements to the tracked ship uncertain.

In conclusion, although the ship-tracking algorithm was intended to increase measurement time and improve the signal-to-noise ratio by averaging multiple measurements over time, it remains challenging in a turbulent and dynamic environment. Nevertheless, it ensures multiple measurements per ship, providing valuable data despite these challenges.

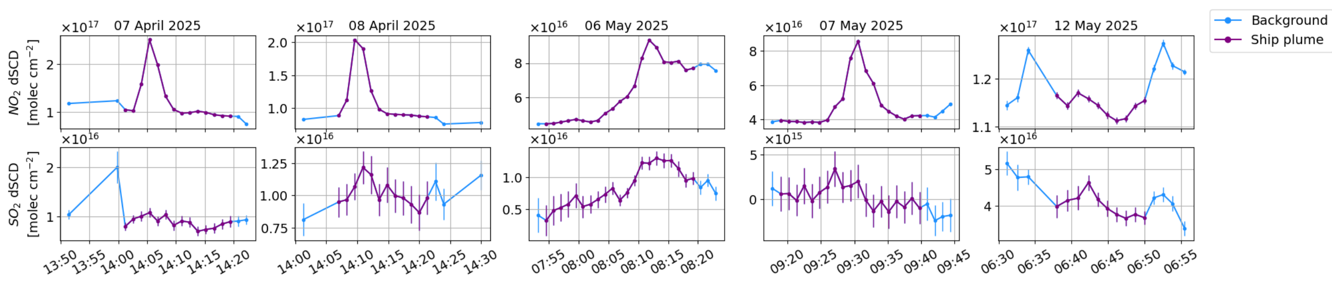

Figure 13. Timeseries of multiple ship tracking case measurements in Zeebrugge with the SEMPAS instrument, averaged over the measurement matrix. Measurements when no ships were in view are indicated in blue, when the ship tracking was active in purple. All measurements are taken at 0.4 degrees elevation, but as the system rotates to track a ship the azimuth angles vary. The measurements without ships are taken at a fixed azimuth: before the measurements at the point where the ship will appear in view, after the measurements at the last azimuth where the ship was tracked.

https://doi.org/10.5194/egusphere-2026-3783
Preprint. Discussion started: 20 August 2026

Figure 14. Measurement matrices for NO_2 shown to scale with respect to the measured ship, during an example ship tracking in Zeebrugge (case 4 in Fig. 13). The shown images correspond to the time at the middle of the acquisition.

5.2 Atmospheric measurements

From MAX-DOAS scans, background concentrations and emissions from other sources than the targeted ships can be quantified. In a heterogeneous port environment such as Zeebrugge, these background levels vary strongly in space and time, complicating the interpretation of ship plume measurements at larger distances. Figure 15 shows MAX-DOAS dSCDs for NO_2, SO_2, HCHO and O_4, coloured by elevation angle for a selection of days at the end of March 2025. Daily timeseries are shown, with a zenith

https://doi.org/10.5194/egusphere-2026-3783
Preprint. Discussion started: 20 August 2026

reference acquired at UTC noon, to highlight the diurnal variation of the trace gases and short-term local enhancements. The data are filtered for a DOAS fit RMS larger than 0.001. As the SO_2 retrieval window is located at shorter wavelengths where the light intensity is lower, it requires sufficient sunlight to achieve an adequate signal-to-noise ratio. As a result, uncertainties increase during the morning and evening hours, and these measurements are filtered out. At solar zenith angles larger than 85°, only zenith measurements are performed.

The collision-induced oxygen complex O_4, is commonly used as indicator for the effective atmospheric lightpath and visibility conditions in MAX-DOAS retrievals (Wagner et al., 2004). Its concentration is predominantly located near Earth's surface and is assumed to be horizontally homogeneously distributed. Variations in O_4 dSCD are dominated by the atmospheric lightpath, such as the presence of clouds and aerosols, and can therefore provide insights in visibility and atmospheric conditions. Under clear-sky conditions, O_4 dSCDs exhibit a characteristic smooth U-shaped diurnal cycle, with enhanced values during morning and evening twilight and a minimum around local noon. This behaviour is caused by changes in the effective atmospheric lightpath length associated with solar zenith angle variations. At high solar zenith angles during sunrise and sunset, photons traverse longer slant paths through the lower atmosphere, increasing the O_4 absorption signal. Around noon, when the sun is highest, the effective lightpath through the troposphere is shortest, resulting in lower O_4 dSCD values. In an optically thin atmosphere with low aerosol loading, the O_4 dSCD is stable. Under such conditions, it can be assumed that single-scattered photons are observed, and the O_4 dSCD value is directly related to the visible range in which the instrument is sensitive.

The NO_2 dSCDs show a similar diurnal dependence, with systematically lower values around noon and higher values in morning and evening. Part of this behaviour is caused by the same geometrical lightpath effects observed in O_4, while an additional contribution arises from photolysis effects related to the atmospheric lifetime of NO_2. Superimposed on this smooth diurnal cycle, short-term enhancements during the day are attributed to tropospheric emissions, either local or transported. The large scatter and rapid variability in the NO_2 dSCDs therefore reflect the highly dynamic nature of local emission sources and changing air mass transport in the port environment. HCHO and SO_2 dSCD variations generally remain limited, despite sporadic emission events coming from the mixed environment.

https://doi.org/10.5194/egusphere-2026-3783
Preprint. Discussion started: 20 August 2026

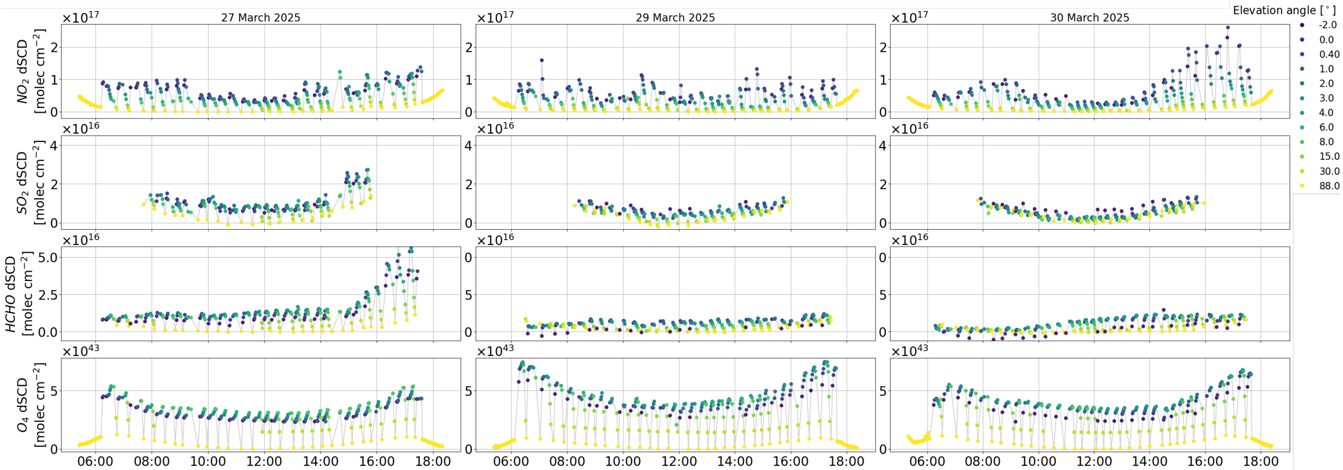

Figure 15. Daily timeseries of trace gases identified in the UV, from atmospheric measurements in the form of MAX-DOAS scans during the Zeebrugge campaign of the SEMPAS instrument. The plots show the diurnal variation and local enhancements of NO_2, SO_2, HCHO and O_4. Three clear-sky days at the end of March 2025 are shown, with time in UTC. The datapoints are coloured by elevation angle and filtered for an RMS of the DOAS fit to be smaller than 0.001. At solar zenith angles larger than 85°, only zenith measurements are taken (in yellow). The zenith reference used in the analysis of the dSCD's is taken daily at the lowest solar zenith angle available, just before noon.

In MAX-DOAS measurements, the elevation angle relates to the effective scattering altitude of the observed molecules. At lower viewing angles, the lightpath traverses dense atmospheric layers, enhancing sensitivity to scattering events closer to the surface. Consequently, measurements at low elevation angles are more sensitive towards absorbers located in the troposphere. In contrast, the vertical lightpath through the stratosphere remains unchanged for all viewing angles. In Fig. 15, this angular dependency translates into a larger scatter of dSCD's at lower viewing angles, dominated by the near-surface emissions. Based on this principle, tropospheric VCDs and profile information per species is derived from the MAX-DOAS scans (Platt and Stutz, 2008). This is accomplished by the FRM4DOAS framework (Sec. 3.2), with the exception of SO_2 analysis not being incorporated in the framework yet.

The port of Zeebrugge is a mixed environment, with sea traffic, industrial port activities and nearby cities. To investigate the origin of the temporal variability in the observations, Fig. 16 shows a wind rose in which the dSCDs of NO_2 and O_4, NO_2 VCDs and near-surface concentrations (NSC) (taken as the lowest layer of the FRM4DOAS profile) are plotted as a function of wind direction. Generally, the largest contribution comes from over land, and overseas emissions are limited. This effect is more pronounced in the dSCDs, both NO_2 and O_4, than in the NO_2 NSC. This indicates the measurements are dominated by lightpath effects: the visibility improves with wind originating from land, compared to winds coming from the sea. As the optical head is pointed towards the sea, sea spray from seaside wind could aid in this effect. The NSC also shows a slight enhancement coming from over land, showing more emissions come from the port and surrounding cities than from ships. The VCDs are more homogeneous, because of vertical mixing. Note that the instrument continuously points towards the sea: these figures are merely indicative and no sources can be distinguished.

https://doi.org/10.5194/egusphere-2026-3783
Preprint. Discussion started: 20 August 2026

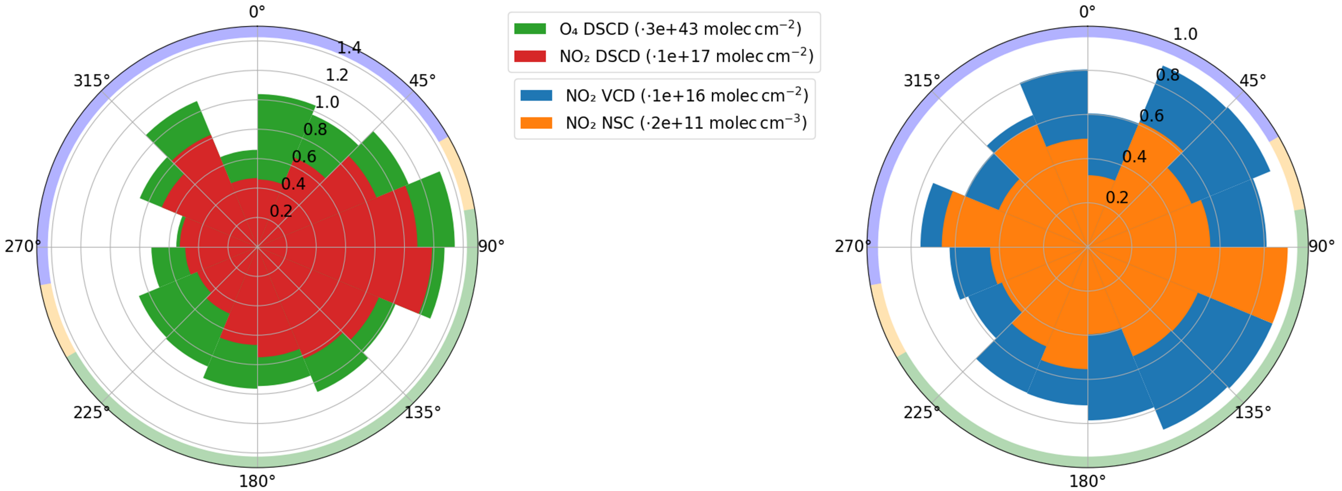

Figure 16. Wind rose showing the direction of the wind at the time of measurement, over the full two month measurement period in Zeebrugge. The surrounding circle shows the origin of the wind: green shows where land is situated, blue indicates sea. Yellow denotes a mixed origin. The left panel shows the dSCDs of NO_2 and O_4 at 1° elevation angle, while the right panel shows NO_2 NSC and VCDs. Note that all species are scaled for visibility.

The NO_2 VCDs of SEMPAS can be compared to the tropospheric NO_2 VCD product of the Sentinel-5P TROPOMI instrument (version 2.08), shown in Fig. 17 and 18. A single SEMPAS measurement at overpass time of the satellite is selected, with a maximum time difference of one hour. The TROPOMI pixels covering a radius of 20 km around the instrument are selected and, if multiple, averaged. VCD uncertainties from the MMF algorithm include measurement and retrieval parameter uncertainties, as well as uncertainties related to aerosol and NO_2 profiles, and those arising from the radiative transfer modelling approach (Friedrich et al., 2019). SEMPAS represents TROPOMI data well at values below 10^{15}. At higher values, SEMPAS often overestimates the NO_2 VCD, for example on 11 April 2025 and 09 May 2025. Local variability such as portal emissions, ships entering and leaving the port, etc. are not captured to the same extent by the satellite instrument as by SEMPAS. The same behaviour is observed in Fig. 18, where lower values correlate well close to the 1-to-1 line, whereas at higher VCDs the values deviate, with higher values for SEMPAS.

https://doi.org/10.5194/egusphere-2026-3783
Preprint. Discussion started: 20 August 2026

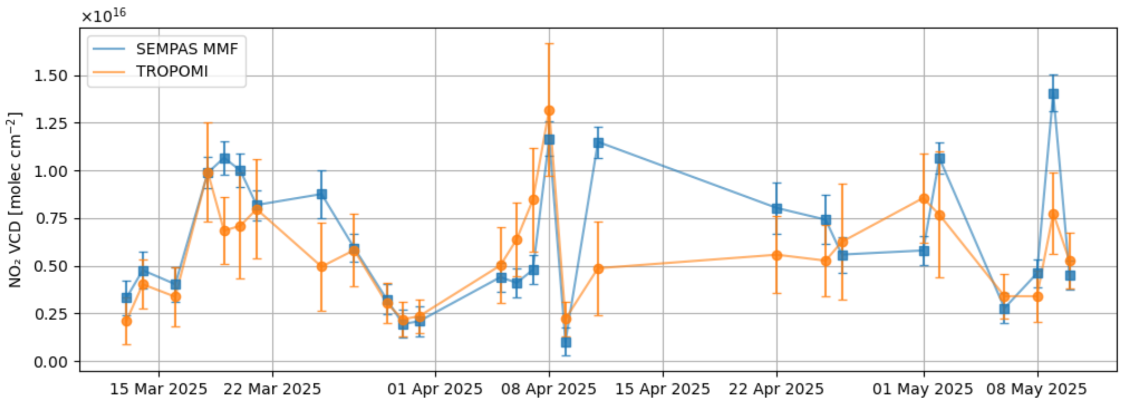

Figure 17. Comparison of SEMPAS NO_2 VCDs as established by the MMF algorithm in the FRM4DOAS framework, with the TROPOMI tropospheric NO_2 column product (version 2.08), over the timespan of the Zeebrugge campaign. The SEMPAS measurement at overpass time is selected, with a maximum time difference of one hour. The TROPOMI measurements covering a radius of 20 km around the instrument are used, and averaged if multiple.

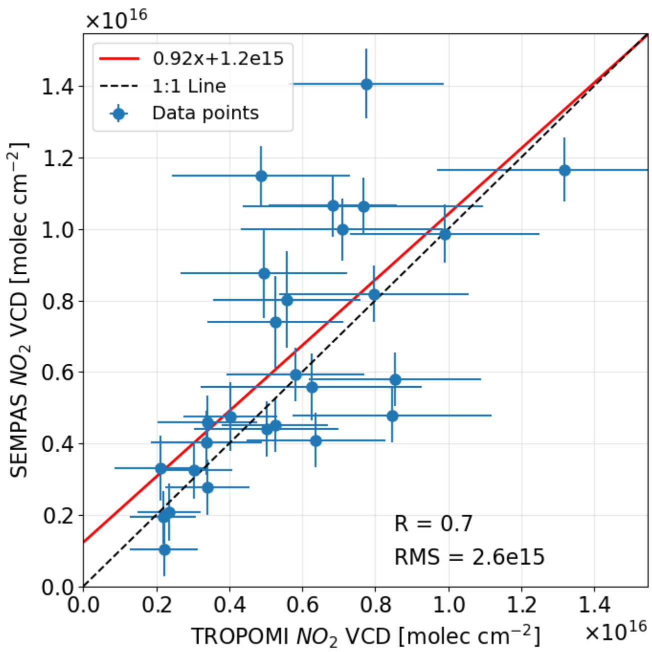

Figure 18. Correlation of the SEMPAS NO_2 VCDs as established by the MMF algorithm in the FRM4DOAS framework, with the TROPOMI tropospheric NO_2 column product (version 2.08), over the timespan of the Zeebrugge campaign. The SEMPAS measurement at overpass time is selected, with a maximum time difference of one hour. The TROPOMI measurements covering a radius of 20 km around the instrument are used, and averaged if multiple.

https://doi.org/10.5194/egusphere-2026-3783
Preprint. Discussion started: 20 August 2026

6 Conclusions & Outlook

This work presents the design, implementation and first measurements of the SEMPAS instrument, an imaging UV-vis spectrometer to monitor shipping emissions. With instrumental straylight reduced, the DOAS spectral fits reach good quality. Detection limits in the order of 5e14 and 1e15 molec/cm^2 are achieved for NO_2 and SO_2 respectively in the binned mode, and approximately four times higher when using bins per fiber, to create the 55 pixels of the image matrix. Robust housing protects the spectrometer and electronics from the marine environment and keeps them in stable conditions. The spectrometer is accompanied by a visible light camera; an algorithm based on YOLO recognition software and a PID-regulator make sure ships can be tracked actively along their trajectory. The ship tracking algorithm is stable and robust, keeping the measurement point constant over time relative to the ship.

The CINDI-3 campaign served as a first test of both the atmospheric monitoring and imaging capabilities of SEMPAS. Results obtained by the SEMPAS MAX-DOAS instrument showed an excellent agreement with the median results of all participating instruments. In the on-shore test campaign in Zeebrugge the ship tracking algorithm was further developed and first ship emission measurements have been demonstrated. In MAX-DOAS mode, retrieved NO_2 VCD's show good agreement with TROPOMI observations, highlighting the potential of SEMPAS for satellite validation over marine environments. The port of Zeebrugge is however a location with highly variable emissions from mixed origin, making it more complex to interpret shipping results. The tracking measurements show the very dynamic nature of the plume emission characteristics: instead of a constant NO_2 and SO_2 value, a variable scene is seen in NO_2, while only weak signals of SO_2 are observed. This is attributed to plume turbulence and dynamics, which makes it challenging to capture the plume continuously.

Next, SEMPAS will be installed off-shore in a Belgian wind turbine park, to measure ships along a major North Sea ship route. Background emissions are expected to be more stable than in a port environment, and the MAX-DOAS mode will provide insights in the atmospheric composition of the marine environment. The turbulent observation scene of the ship plume will be studied in more detail, disentangling its dynamics. Measurements with shorter integration time could be opted for, providing a higher temporal variability, at the cost of sensitivity. In this case, the NO_2 plume could be mapped more clearly, before defining the best strategy for SO_2 measurements as well. With an optimal tracking strategy and well-understood observation scene, the objective is to define emission factors of the measured ships based on NO_2 and SO_2 dSCD's and ship and environmental parameters. To reach this, an excess value per plume above its local background needs to be quantified. Next steps in this project will characterise better the conditions under which good measurements are possible and their limiting factors, both for NO_2 and SO_2. As a pilot project, SEMPAS takes a step towards more systematic compliance monitoring in the NECA and SECA control areas. Based on the observed emission factors, more targeted control measures could be taken and the environmental impact of shipping can be reduced.

In the longer term, a plume dispersion model could be coupled to the measurements, to identify the location and extent of the core region in the plume a priori. The PID-regulator could be replaced by a more complicated regulation model to limit oscillations and residual errors. A different detector could be introduced to bring more fibers into view and generate larger images. Future work could explore opportunities for multiple installation locations, to cover a broader network of ship

https://doi.org/10.5194/egusphere-2026-3783
Preprint. Discussion started: 20 August 2026

routes. An iteration of SEMPAS instruments, may further improve optical, mechanical and software design, facilitating wider deployment and enhanced observational capabilities.

Author contributions. Gytha Mettepenningen: development of the instrument in the lab and during test campaigns (hardware and software), data analysis, writing. Michel Van Roozendael: supervision, support and guidance during development of the instrument and data analysis, conceptualisation, editing. Caroline Fayt: software development. Cato Van Doorne & Lars Jacobs: mechanical housing development. Aurélien Aubry & Timo Van Laar & Sophie Berkenbosch: electronical housing development. Frederik Tack: scientific discussion, conceptualisation, editing. Martine De Mazière: conceptualisation, scientific discussion. Eddy Neefs: conceptualisation. Filip Desmet: scientific discussion. Clemens Mensink: supervision.

Competing interests. Michel Van Roozendael is member of the editorial board of Atmospheric Measurement Techniques. The authors declare that they have no further conflict of interest.

Acknowledgements. We gratefully acknowledge the Belgian FPS Health, Food Chain Safety and Environment and DG Shipping for funding and supporting the project. The authors would like to thank the colleagues in the UV-visible observations group of BIRA-IASB for their support during the development of the instrument, especially Alexis Merlaud for instrumental support, Martina Friedrich for software support, Gaia Pinardi for providing the TROPOMI data and the engineering department for technical support. AI was used to correct spelling and improve code for generating figures.

Code/Data availibility. The data acquired by SEMPAS presented in the results of this paper is published on BIRA-IASB's data repository and can be accessed through https://doi.org/10.18758/iybb1vnm (Mettepenningen et al., 2026). Code is available upon request.

Video supplements. The supplementary material contains a video of a ship tracking result, according to Fig. 11. This video can be found at https://doi.org/10.5446/73638 in the Leibniz Information Centre for Science and Technology University Library.

https://doi.org/10.5194/egusphere-2026-3783
Preprint. Discussion started: 20 August 2026

References

Alföldy, B., Lööv, J. B., Lagler, F., Mellqvist, J., Berg, N., Beecken, J., Weststrate, H., Duyzer, J., Bencs, L., Horemans, B., Cavalli, F., Putaud, J.-P., Janssens-Maenhout, G., Csordás, A. P., Van Grieken, R., Borowiak, A., and Hjorth, J.: Measurements of air pollution emission factors for marine transportation in SECA, Atmospheric Measurement Techniques, 6, 1777–1791, https://doi.org/https://doi.org/10.5194/amt-6-1777-2013, 2013.

Aulinger, A. et al.: The impact of shipping emissions on air pollution in the greater North Sea region – Part 1: Current emissions and concentrations, Atmospheric Chemistry and Physics, 16, 10 997–11 023, 2016.

Balzani Lööv, J. M., Alfoldy, B., Gast, L. F. L., Hjorth, J., Lagler, F., Mellqvist, J., Beecken, J., Berg, N., Duyzer, J., Westrate, H., Swart, D. P. J., Berkhout, A. J. C., Jalkanen, J.-P., Prata, A. J., Van Der Hoff, G. R., and Borowiak, A.: Field test of available methods to measure remotely SO_x and NO_x emissions from ships, Atmospheric Measurement Techniques, 7, 2597–2613, https://doi.org/https://doi.org/10.5194/amt-7-2597-2014, 2014.

Beecken, J., Weigelt, A., Griesel, S., Mellqvist, J., Conde, A. V., Van Dinther, D., Duyzer, J., Knudsen, J., Knudsen, B., and Ntziachristos, L.: Performance assessment of state-of-the-art and novel methods for remote compliance monitoring of sulphur emissions from shipping, https://doi.org/https://doi.org/10.5194/amt-2023-93, 2023.

Beirle, S., Dörner, S., Donner, S., Remmers, J., Wang, Y., and Wagner, T.: The Mainz profile algorithm (MAPA), Atmospheric Measurement Techniques, 12, 1785–1806, https://doi.org/https://doi.org/10.5194/amt-12-1785-2019, 2019.

Berg, N., Mellqvist, J., Jalkanen, J.-P., and Balzani, J.: Ship emissions of SO_2 and NO_2: DOAS measurements from airborne platforms, Atmospheric Measurement Techniques, 5, 1085–1098, https://doi.org/https://doi.org/10.5194/amt-5-1085-2012, 2012.

Carpenter, L. J., Fleming, Z. L., Read, K. A., Lee, J. D., Moller, S. J., Hopkins, J. R., Purvis, R. M., Lewis, A. C., Müller, K., Heinold, B., Herrmann, H., Wadinga Fomba, K., van Pinxteren, D., Müller, C., Tegen, I., Wiedensohler, A., Müller, T., Niedermeier, N., Achterberg, E. P., Patey, M. D., Kozlova, E. A., Heimann, M., Heard, D. E., Plane, J. M. C., Mahajan, A., Oetjen, H., Ingham, T., Stone, D., Whalley, L. K., Evans, M. J., Pilling, M. J., Leigh, R. J., Monks, P. S., Karunaharan, A., Vaughan, S., Arnold, S. R., Tschritter, J., Pöhler, D., Frieß, U., Holla, R., Mendes, L. M., Lopez, H., Faria, B., Manning, A. J., and Wallace, D. W. R.: Seasonal characteristics of tropical marine boundary layer air measured at the Cape Verde Atmospheric Observatory, Journal of Atmospheric Chemistry, 67, 87–140, https://doi.org/https://doi.org/10.1007/s10874-011-9206-1, 2010.

Chance, K. and Kurucz, R. L.: An improved high-resolution solar reference spectrum for Earth's atmosphere measurements in the ultraviolet, visible, and near infrared (SAO2010), Journal of Quantitative Spectroscopy and Radiative Transfer, 111, 1289–1295, https://doi.org/https://doi.org/10.1016/j.jqsrt.2010.01.036, 2010.

Cheng, C.-W., Hua, J., and Hwang, D.-S.: NO_x emission calculations for bulk carriers by using engine power probabilities as weighting factors, Journal of the Air and Waste Management Association, 67, 1146–1157, https://doi.org/https://doi.org/10.1080/10962247.2017.1356763, 2017.

Cheng, Y., Wang, S., Zhu, J., Guo, Y., Zhang, R., Liu, Y., Zhang, Y., Yu, Q., Ma, W., and Zhou, B.: Surveillance of SO_2 and NO_2 from ship emissions by MAX-DOAS measurements and the implications regarding fuel sulfur content compliance, Atmospheric Chemistry and Physics, 19, 13 611–13 626, https://doi.org/https://doi.org/10.5194/acp-19-13611-2019, 2019.

Danckaert, T., Fayt, C., Van Roozendael, M., De Smedt, I., Letocart, V., Merlaud, A., and Pinardi, G.: QDOAS Software user manual, Tech. rep., Royal Belgian Institute for Space Aeronomy, 2017.

https://doi.org/10.5194/egusphere-2026-3783
Preprint. Discussion started: 20 August 2026

Eyring, V., Köhler, H. W., van Aardenne, J., and Lauer, A.: Emissions from international shipping: 1. The last 50 years, Journal of Geophysical Research: Atmospheres, 110, https://doi.org/https://doi.org/10.1029/2004JD005619, 2005.

Finkenzeller, H. and Volkamer, R.: O_2–O_2 CIA in the gas phase: Cross-section of weak bands, and continuum absorption between 297–500 nm, Journal of Quantitative Spectroscopy and Radiative Transfer, 279, 108 063, https://doi.org/https://doi.org/10.1016/j.jqsrt.2021.108063, 2022.

Fleischmann, O. C., Hartmann, M., Burrows, J. P., and Orphal, J.: New ultraviolet absorption cross-sections of BrO at atmospheric temperatures measured by time-windowing Fourier-transform spectroscopy, Journal of Photochemistry and Photobiology A: Chemistry, 168, 117–132, https://doi.org/https://doi.org/10.1016/j.jphotochem.2004.03.026, 2004.

Friedrich, M. M., Rivera, C., Stremme, W., Ojeda, Z., Arellano, J., Bezanilla, A., García-Reynoso, J. A., and Grutter, M.: NO2 vertical profiles and column densities from MAX-DOAS measurements in Mexico City, Atmospheric Measurement Techniques, 12, 2545–2565, https://doi.org/https://doi.org/10.5194/amt-12-2545-2019, 2019.

Gramme, P., Busschots, C., Dekemper, E., Pieroux, D., Baker, N., Casadio, S., Iannarelli, A. M., Ferrante, N., Bernardino, A. D., Pettinari, P., Castelli, E., di Liberto, L., and Cairo, F.: Urban pollution monitoring with the AOTF-based NO2 camera: validation with other DOAS instruments, Atmospheric Measurement Techniques, 18, 6021–6037, https://doi.org/https://doi.org/10.5194/amt-18-6021-2025, 2025.

Hakkarainen, J., Kuhlmann, G., Koene, E., Santaren, D., Meier, S., Krol, M. C., van Stratum, B. J., Ialongo, I., Chevallier, F., Tamminen, J., Brunner, D., and Broquet, G.: Analyzing nitrogen dioxide to nitrogen oxide scaling factors for data-driven satellite-based emission estimation methods: A case study of Matimba/Medupi power stations in South Africa, Atmospheric Pollution Research, 15, 102 171, https://doi.org/https://doi.org/10.1016/j.apr.2024.102171, 2024.

Hönninger, G., von Friedeburg, C., and Platt, U.: Multi axis differential optical absorption spectroscopy (MAX-DOAS), Atmospheric Chemistry and Physics, 4, 231–254, https://doi.org/https://doi.org/10.5194/acp-4-231-2004, 2004.

Krause, K., Wittrock, F., Richter, A., Schmitt, S., Pöhler, D., Weigelt, A., and Burrows, J. P.: Estimation of ship emission rates at a major shipping lane by long-path DOAS measurements, Atmospheric Measurement Techniques, 14, 5791–5807, https://doi.org/https://doi.org/10.5194/amt-14-5791-2021, 2021.

Kreher, K., Van Roozendael, M., Hendrick, F., Apituley, A., Dimitropoulou, E., Frieß, U., Richter, A., Wagner, T., Lampel, J., Abuhassan, N., Ang, L., Anguas, M., Bais, A., Benavent, N., Bösch, T., Bognar, K., Borovski, A., Bruchkouski, I., Cede, A., Chan, K. L., Donner, S., Drosoglou, T., Fayt, C., Finkenzeller, H., Garcia-Nieto, D., Gielen, C., Gómez-Martín, L., Hao, N., Henzing, B., Herman, J. R., Hermans, C., Hoque, S., Irie, H., Jin, J., Johnston, P., Khayyam Butt, J., Khokhar, F., Koenig, T. K., Kuhn, J., Kumar, V., Liu, C., Ma, J., Merlaud, A., Mishra, A. K., Müller, M., Navarro-Comas, M., Ostendorf, M., Pazmino, A., Peters, E., Pinardi, G., Pinharanda, M., Piters, A., Platt, U., Postylyakov, O., Prados-Roman, C., Puentedura, O., Querel, R., Saiz-Lopez, A., Schönhardt, A., Schreier, S. F., Seyler, A., Sinha, V., Spinei, E., Strong, K., Tack, F., Tian, X., Tiefengraber, M., Tirpitz, J.-L., Van Gent, J., Volkamer, R., Vrekoussis, M., Wang, S., Wang, Z., Wenig, M., Wittrock, F., Xie, P. H., Xu, J., Yela, M., Zhang, C., and Zhao, X.: Intercomparison of NO_2, O_4, O_3 and HCHO slant column measurements by MAX-DOAS and zenith-sky UV–visible spectrometers during CINDI-2, Atmospheric Measurement Techniques, 13, 2169–2208, https://doi.org/https://doi.org/10.5194/amt-13-2169-2020, 2020.

Lawrence, J. P., Anand, J. S., Vande Hey, J. D., White, J., Leigh, R. R., Monks, P. S., and Leigh, R. J.: High-resolution measurements from the airborne Atmospheric Nitrogen Dioxide Imager (ANDI), Atmospheric Measurement Techniques, 8, 4735–4754, https://doi.org/https://doi.org/10.5194/amt-8-4735-2015, 2015.

https://doi.org/10.5194/egusphere-2026-3783
Preprint. Discussion started: 20 August 2026

Manshausen, P., Watson-Parris, D., Christensen, M., Jalkanen, J.-P., and Stier, P.: New analysis of shipping emissions reveals that air pollution has a larger effect on climate than previously thought, Nature, 610, 101–106, https://doi.org/https://doi.org/10.1038/s41586-022-05122-0, 2022.

Meller, R. and Moortgat, G. K.: Temperature dependence of the absorption cross sections of formaldehyde between 223 and 323 K in the wavelength range 225–375 nm, Journal of Geophysical Research: Atmospheres, 105, 7089–7102, https://doi.org/https://doi.org/10.1029/1999JD901074, 2000.

Mellqvist, J. and Conde, V.: Best practice report on compliance monitoring of ships with respect to current and future IMO regulation, 2021.

MEPC: Amendments to the Technical Code on Control of Emission of Nitrogen Oxides from Marine Diesel Engines, Resolution MEPC.177(58), Adopted on 10 October 2008 (NO. Technical Code 2008), Tech. rep., IMO, 2008.

MEPC: Amendments to the Annex of the Protocol of 1997 to Amend the International Convention for the Prevention of Pollution from Ships, 1973, as Modified by the Protocol of 1978 Relating Thereto (2021 Revised MARPOL Annex VI), Resolution MEPC.328(76), Entered into Force on 1 November 2022, Tech. rep., IMO, 2022.

MEPC: List of Special Areas, Emission Control Areas and Particularly Sensitive Sea Areas, Circular MEPC.1/Circ.778/Rev.3 of 9 May 2025, Tech. rep., IMO, 2025.

Mettepenningen, G., Van Roozendael, M., and Fayt, C.: L2 data from the SEMPAS instrument in Zeebrugge, Belgium, https://doi.org/https://doi.org/10.18758/iybb1vnm, 2026.

Moreira, C. A. B., Polezer, G., dos Santos Silva, J. C., de Souza Zorzenão, P. C., Godoi, A. F. L., Huergo, L. F., Yamamoto, C. I., de Souza Tadano, Y., Potgieter-Vermaak, S., Reis, R. A., Oliveira, A., and Godoi, R. H. M.: Impact assessment of IMO's sulfur content limits: a case study at Latin America's largest grain port, Air Quality, Atmosphere and Health, 17, 2337–2351, https://doi.org/https://doi.org/10.1007/s11869-024-01576-5, 2024.

Peters, E., Ostendorf, M., Bösch, T., Seyler, A., Schönhardt, A., Schreier, S. F., Henzing, J. S., Wittrock, F., Richter, A., Vrekoussis, M., and Burrows, J. P.: Full-azimuthal imaging-DOAS observations of NO_2 and O_4 during CINDI-2, Atmospheric Measurement Techniques, 12, 4171–4190, https://doi.org/https://doi.org/10.5194/amt-12-4171-2019, 2019.

Platt, U. and Stutz, J.: Differential Optical Absorption Spectroscopy, Springer, ISBN 978-3-540-21193-8, 2008.

Repka, S., Erkkilä-Välimäki, A., Jonson, J. E., Posch, M., Törrönen, J., and Jalkanen, J. P.: Assessing the costs and environmental benefits of IMO regulations of ship-originated SOx and NOx emissions in the Baltic Sea, Ambio, 50, 1718–1730, https://doi.org/https://doi.org/10.1007/s13280-021-01500-6, 2021.

Riess, T.: Spaceborne monitoring of nitrogen oxides emissions from ships with TROPOMI, Ph.D. thesis, Wageningen University and Research, https://doi.org/https://doi.org/10.18174/671443, 2024.

Rothman, L., Gordon, I., Babikov, Y., Barbe, A., Benner, D. C., Bernath, P., Birk, M., Bizzocchi, L., Boudon, V., Brown, L., Campargue, A., Chance, K., Cohen, E., Coudert, L., Devi, V., Drouin, B., Fayt, A., Flaud, J.-M., Gamache, R., Harrison, J., Hartmann, J.-M., Hill, C., Hodges, J., Jacquemart, D., Jolly, A., Lamouroux, J., Le Roy, R., Li, G., Long, D., Lyulin, O., Mackie, C., Massie, S., Mikhailenko, S., Müller, H., Naumenko, O., Nikitin, A., Orphal, J., Perevalov, V., Perrin, A., Polovtseva, E., Richard, C., Smith, M., Starikova, E., Sung, K., Tashkun, S., Tennyson, J., Toon, G., Tyuterev, V., and Wagner, G.: The HITRAN2012 molecular spectroscopic database, Journal of Quantative Spectroscopy and Radiative Transfer, 130, 4–50, https://doi.org/https://doi.org/10.1016/j.jqsrt.2013.07.002, 2013.

Schreier, S. F., Peters, E., Richter, A., Lampel, J., Wittrock, F., and Burrows, J. P.: Ship-based MAX-DOAS measurements of tropospheric NO2 and SO2 in the South China and Sulu Sea, Atmospheric Environment, 102, 331–343, https://doi.org/https://doi.org/10.1016/j.atmosenv.2014.12.015, 2015.

https://doi.org/10.5194/egusphere-2026-3783
Preprint. Discussion started: 20 August 2026

Serdyuchenko, A., Gorshelev, V., Weber, M., Chehade, W., and Burrows, J. P.: High spectral resolution ozone absorption cross-sections – Part 2: Temperature dependence, Atmos. Meas. Tech., 7, 625–636, https://doi.org/https://doi.org/10.5194/amt-7-625-2014, 2014.

Seyler, A., Wittrock, F., Kattner, L., Mathieu-Üffing, B., Peters, E., Richter, A., Schmolke, S., and Burrows, J. P.: Monitoring shipping emissions in the German Bight using MAX-DOAS measurements, Atmospheric Chemistry and Physics, 17, 10 997–11 023, https://doi.org/https://doi.org/10.5194/acp-17-10997-2017, 2017.

Tack, F., Merlaud, A., Iordache, M.-D., Danckaert, T., Yu, H., Fayt, C., Meuleman, K., Deutsch, F., Fierens, F., and Van Roozendael, M.: High-resolution mapping of the NO_2 spatial distribution over Belgian urban areas based on airborne APEX remote sensing, Atmospheric Measurement Techniques, 10, 1665–1688, https://doi.org/https://doi.org/10.5194/amt-10-1665-2017, 2017.

Tan, W., Liu, C., Wang, S., Xing, C., Su, W., Zhang, C., Xia, C., Liu, H., Cai, Z., and Liu, J.: Tropospheric NO2, SO2, and HCHO over the East China Sea, using ship-based MAX-DOAS observations and comparison with OMI and OMPS satellite data, Atmospheric Chemistry and Physics, 18, 15 387–15 402, https://doi.org/https://doi.org/10.5194/acp-18-15387-2018, 2018.

Van Roozendael, M., Hendrick, F., Friedrich, M. M., Fayt, C., Bais, A., Beirle, S., Bösch, T., Navarro Comas, M., Friess, U., Karagkiozidis, D., Kreher, K., Merlaud, A., Pinardi, G., Piters, A., Prados-Roman, C., Puentedura, O., Reischmann, L., Richter, A., Tirpitz, J.-L., Wagner, T., Yela, M., and Ziegler, S.: Fiducial Reference Measurements for Air Quality Monitoring Using Ground-Based MAX-DOAS Instruments (FRM4DOAS), Remote Sensing, 16, 4523, https://doi.org/https://doi.org/10.3390/rs16234523, 2024.

Van Roy, W., Scheldeman, K., Van Roozendael, B., Van Nieuwenhove, A., Schallier, R., Vigin, L., and Maes, F.: Airborne monitoring of compliance to NOx emission regulations from ocean-going vessels in the Belgian North Sea, Atmospheric Pollution Research, 13, 101 518, https://doi.org/https://doi.org/10.1016/j.apr.2022.101518, 2022.

Van Roy, W., Van Nieuwenhove, A., Scheldeman, K., Van Roozendael, B., Schallier, R., Mellqvist, J., and Maes, F.: Measurement of Sulfur-Dioxide Emissions from Ocean-Going Vessels in Belgium Using Novel Techniques, Atmosphere, 13, 1756, https://doi.org/https://doi.org/10.3390/atmos13111756, 2022.

Vandaele, A. C., Hermans, C., Simon, P. C., Carleer, M., Colin, R., Fally, S., Mérienne, M. F., Jenouvrier, A., and Coquart, B.: Measurements of the NO_2 absorption cross-section from 42 000 cm^{-1} to 10 000 cm^{-1} (238–1000 nm) at 220 K and 294 K, Journal of Quantitative Spectroscopy and Radiative Transfer, 59, 171–184, https://doi.org/https://doi.org/10.1016/S0022-4073(97)00168-4, 1998.

Vandaele, A. C., Hermans, C., and Fally, S.: Fourier transform measurements of SO_2 absorption cross sections: II. Temperature dependence in the 29 000–44 000 cm^{-1} (227–345 nm) region, Journal of Quantitative Spectroscopy and Radiative Transfer, 110, 2115–2126, https://doi.org/https://doi.org/10.1016/j.jqsrt.2009.05.006, 2009.

Wagner, T., Dix, B., von Friedeburg, C., Friess, U., Sanghavi, S., Sinreich, R., and Platt, U.: MAX-DOAS O4 measurements: A new technique to derive information on atmospheric aerosols — Principles and information content, Journal of Geophysical Research, 109, 22 205, https://doi.org/https://doi.org/10.1029/2004JD004904, 2004.

Wang, P., Piters, A., van Geffen, J., Tuinder, O., Stammes, P., and Kinne, S.: Shipborne MAX-DOAS measurements for validation of TROPOMI NO2 products, Atmospheric Measurement Techniques, 13, 1413–1426, https://doi.org/https://doi.org/10.5194/amt-13-1413-2020, 2020.

Wang, T., Hendrick, F., Wang, P., Tang, G., Clémer, K., Yu, H., Fayt, C., Hermans, C., Gielen, C., Müller, J.-F., Pinardi, G., Theys, N., Brenot, H., and Van Roozendael, M.: Evaluation of tropospheric SO_2 retrieved from MAX-DOAS measurements in Xianghe, China, Atmospheric Chemistry and Physics, 14, 11 149–11 164, https://doi.org/https://doi.org/10.5194/acp-14-11149-2014, 2014.

https://doi.org/10.5194/egusphere-2026-3783
Preprint. Discussion started: 20 August 2026

Wittrock, F., Oetjen, H., Richter, A., Fietkau, S., Medeke, T., Rozanov, A., and Burrows, J. P.: MAX-DOAS measurements of atmospheric trace gases in Ny-Ålesund – Radiative transfer studies and their application, Atmospheric Chemistry and Physics, 4, 955–966, https://doi.org/https://doi.org/10.5194/acp-4-955-2004, 2004.

Yang, M., Bell, T. G., Hopkins, F. E., and Smyth, T. J.: Attribution of atmospheric sulfur dioxide over the English Channel to dimethyl sulfide and changing ship emissions, Atmospheric Chemistry and Physics, 16, 4771–4783, https://doi.org/https://doi.org/10.5194/acp-16-4771-2016, 2016.

Zong, Y., Brown, S. W., Johnson, B. C., Lykke, K. R., and Ohno, Y.: Simple spectral stray light correction method for array spectroradiometers, Applied Optics, 45, 1111–1119, https://doi.org/https://doi.org/10.1364/AO.45.001111, 2006.